

1 **Biological production in two contrasted regions of the Mediterranean Sea during the**
2 **oligotrophic period: An estimate based on the diel cycle of optical properties measured by**
3 **BGC-Argo profiling floats**

4 Marie Barbieux¹, Julia Uitz¹, Alexandre Mignot², Collin Roesler³, Hervé Claustre¹, Bernard
5 Gentili¹, Vincent Taillandier¹, Fabrizio D'Ortenzio¹, Hubert Loisel⁴, Antoine Poteau¹, Edouard
6 Leymarie¹, Christophe Penkerc'h¹, Catherine Schmechtig⁵, Annick Bricaud¹

7 ¹CNRS and Sorbonne Université, Laboratoire d'Océanographie de Villefranche, LOV, 06230 Villefranche-sur-
8 Mer, France

9 ²Mercator Océan, 31520 Ramonville-Saint-Agne, France

10 ³Bowdoin College, Earth and Oceanographic Science, Brunswick, Maine 04011, USA

11 ⁴Université Littoral Côte d'Opale, Université Lille, CNRS, Laboratoire d'Océanologie et de Géosciences, 59000
12 Lille, France

13 ⁵OSU Ecce Terra, UMS 3455, CNRS and Sorbonne Université, Paris 6, 4 place Jussieu, 75252 Paris CEDEX 05,
14 France

15 Correspondence to: J. Uitz (julia.uitz@imev-mer.fr)

16

17 **Abstract**

18 This study assesses marine **community** production based on the diel variability of bio-
19 optical properties monitored by two BioGeoChemical-Argo (BGC-Argo) floats. Experiments
20 were conducted in two distinct Mediterranean systems, the Northwestern Ligurian Sea and the
21 Central Ionian Sea, during summer months. We derived particulate organic carbon (POC) stock
22 and gross community production integrated within the surface, euphotic and subsurface
23 chlorophyll maximum (SCM) layers, using an existing approach applied to diel cycle
24 measurements of the particulate beam attenuation (c_p) and backscattering (b_{bp}) coefficients. The
25 diel cycle of c_p provided a robust proxy for quantifying biological production in both systems;
26 that of b_{bp} was comparatively less robust. Derived primary production estimates vary by a factor
27 of 2 depending upon the choice of the bio-optical relationship that converts the measured optical
28 coefficient to POC, which is thus a critical step to constrain. Our results indicate a substantial
29 **contribution to the water column production of the SCM layer (16–42%), that varies largely**
30 **with the considered system.** In the Ligurian Sea, the SCM is a seasonal feature that behaves as
31 a subsurface biomass maximum (SBM) with the ability to respond to episodic abiotic forcing
32 by increasing production. In contrast, in the Ionian Sea, the SCM is permanent, **primarily**
33 induced by phytoplankton photoacclimation and contributes moderately to water column
34 production. These results **clearly demonstrate** the strong potential for transmissometers
35 deployed on BGC-Argo profiling floats to quantify non-intrusively *in situ* biological production
36 of organic carbon in the water column of stratified oligotrophic systems with recurring or
37 permanent SCMs, which are widespread features in the global ocean.

38

a supprimé: biological
a supprimé: of organic carbon

a supprimé: , yet variable,

a supprimé: emphasize

43 1 Introduction

44 Primary production is an essential process in the global ocean carbon cycle (Field et al.
45 1998). As a major driver of the biological carbon pump, this biogeochemical process plays a
46 critical role in the regulation of the Earth's climate (e.g. Sarmiento & Siegenthaler 1992;
47 Falkowski 2012). Hence, quantifying primary production as a function of time and space in the
48 ocean stands as a major challenge in the context of climate change. The balance between gross
49 primary production and community respiration in the ocean determines the trophic status of
50 marine systems, i.e. whether the system acts as a source or a sink of carbon (Williams 1993).
51 This balance depends on the considered region and varies substantially according to spatial and
52 temporal scales (Geider et al. 1997; Duarte & Agusti 1998; del Giorgio & Duarte 2002). It is
53 therefore necessary to develop capabilities not only for assessing primary production on a
54 global scale, but also for characterizing and quantifying the biogeochemical functioning of
55 marine ecosystems at smaller spatial and temporal scales (Serret et al. 1999; González et al.
56 2001 & 2002).

57 Traditionally, primary production measurements are based on *in situ* or *in vitro* incubation
58 experiments (i.e. on board the ship, under controlled conditions) coupled with isotopic carbon
59 analysis (Nielsen 1952; Fitzwater et al. 1982; Dandonneau 1993; Barber & Hitling 2002) or
60 measurements of oxygen concentration (Williams & Jenkinson 1982; Williams & Purdie 1991).
61 These methods involve seawater sampling during field campaigns, sample manipulation and
62 subsequent laboratory analyses, which are both time consuming and require strong technical
63 expertise. As a result, the availability of field primary production measurements is relatively
64 limited in terms of spatial and temporal coverage, which hinders the possibility of extrapolation
65 to other systems or to larger space and time scales for modeling purposes. Active chlorophyll
66 fluorescence techniques, such as Fast Repetition Rate Fluorometry (FRRF), yield in situ
67 phytoplankton physiological parameters, which when combined with appropriate modeling,

a supprimé: component

a supprimé: of

70 provide estimates of derive primary production (e.g. Kolber & Falkowski 1993; Smyth et al.
71 2004). This technique has the major advantage of providing an instantaneous, fine-scale
72 estimation of primary production in a non-invasive manner. Nevertheless, it is subject to
73 assumptions and uncertainties, in particular related to the interpretation of fluorescence-light
74 curve information in terms of carbon fixation, that still limit its use (see., e.g., Suggett et al.
75 2004; Corno et al. 2005; Regaudie-de-Gioux et al. 2014 and references herein).

76 Bio-optical primary production models coupled with ocean color satellite imagery
77 represent another approach for obtaining primary production estimates (Morel 1991; Longhurst
78 et al. 1995; Antoine et al. 1996; Behrenfeld et al. 2002). Such models are extremely valuable
79 for assessing primary production with a large spatial coverage and over a broad range of
80 temporal scales (Sathyendranath et al. 1995; Uitz et al. 2010; Chavez et al. 2011). Yet, most of
81 these models suffer from several sources of uncertainty, that can generate potential errors in the
82 production estimates (e.g. Sarmiento et al. 2004; Saba et al. 2010; Saba et al. 2011). Sources of
83 uncertainty include, in particular, the extrapolation of the satellite chlorophyll product, which
84 is weighted to the upper portion of the euphotic zone, to the entirety of the productive region
85 of the water column not sensed remotely. In addition, the *in situ*-based parameterization of
86 phytoplankton photophysiology tends to lack robustness when applied to large (regional or
87 global) scales and over seasonal to interannual time scales.

88 Diel cycles observed in bio-optical properties provide a less-empirical and more
89 mechanistic approach to assess biological production. In a seminal paper published in 1989,
90 Siegel et al. observed the *in situ* diurnal variability of the particulate beam attenuation
91 coefficient (c_p) and used it as a surrogate for the diurnal variations in the abundance of biogenic
92 particles and associated production in the oligotrophic North Pacific Ocean. Several studies
93 subsequently pursued the investigation of the diurnal variability of marine bio-optical properties
94 as a means for determining non-intrusively *in situ* biological production (e.g. Stramska &

a supprimé: ies

a supprimé: ies

97 Dickey 1992; Durand and Olson 1996; Claustre et al. 1999; Claustre 2008; Gernez et al. 2011;
98 White et al. 2017; Briggs et al. 2018).

99 Among this large body of literature, Claustre et al. (2008) carried further the principle of
100 the Siegel et al. (1989) approach for application to the South Pacific Subtropical Ocean. Based
101 upon the generally observed relationship between the c_p coefficient and the stock of particulate
102 organic carbon, POC (e.g. Stramski et al. 1999; Garner et al. 2006), Claustre et al. (2008)
103 assumed that diel variations in c_p reflect diel variations in POC. Thus, the observed daytime
104 increase and nighttime decrease in c_p -derived POC are used to estimate gross community
105 production, community losses and, assuming equivalent day and night losses, net community
106 production. Because the c_p coefficient is not specific to phytoplankton but includes the POC
107 contribution of both autotrophic and heterotrophic particles, the c_p -based method yields
108 estimate of community production.

109 Two studies (Kheireddine & Antoine 2014; Barnes & Antoine 2014) extended the
110 approach to the particulate backscattering coefficient (b_{bp}). The application opens up
111 opportunities for assessing community production from geostationary ocean color satellite
112 observations, from which a nearly continuous daytime b_{bp} coefficient can be retrieved. Both
113 studies focused on surface data obtained from moored observations from the Ligurian Sea
114 (Northwestern Mediterranean) and found that the diel cycle of b_{bp} may not necessarily be
115 interchanged with that of c_p , which calls for further investigations.

116 The optics-based approach has proven to be particularly relevant for appraising
117 particulate biological production in stratified oligotrophic systems such as subtropical gyres
118 (e.g. Siegel et al. 1998; Claustre et al. 2008; White et al. 2017). Interestingly, in such systems,
119 the biological production of organic carbon is difficult to quantify and potentially
120 underestimated by ^{14}C incubation methods (Juraneck & Quay 2005; Quay et al. 2010). This
121 might be attributed to an inadequacy of traditional measurement methods for adequately

a supprimé: also attempted to

a supprimé: is

a supprimé: weak

a supprimé: results for

a supprimé: cycle

a supprimé: ,

a supprimé: ing

a supprimé: apprehending

130 capturing the spatial and temporal heterogeneity of biological production that may exhibit local
131 or episodic events (Karl et al. 2003; Williams et al. 2004; McGillicuddy 2016). Moreover, in
132 stratified oligotrophic systems, the vertical distribution of phytoplankton is frequently
133 characterized by the presence of a deep chlorophyll maximum (DCM), also referred as
134 subsurface chlorophyll maximum (SCM; e.g. Cullen 1982; Hense & Beckmann 2008; Cullen
135 2015; Mignot et al., 2014). SCMs are not necessarily resolved by *in situ* discrete sampling and
136 cannot be observed from ocean color satellites that are limited to the surface ocean. They are
137 typically attributed to phytoplankton photoacclimation, the physiological process by which
138 phytoplankton cells adjust to light limitation by increasing their intracellular chlorophyll
139 content without concomitant increase in carbon (Kiefer et al. 1976; Cullen 1982; Fennel & Boss
140 2003; Letelier et al., 2004; Dubinsky & Stambler 2009). Yet, SCMs resulting from an actual
141 increase in phytoplankton (carbon) biomass, and so referred to as subsurface biomass maximum
142 (SBM), have also been observed episodically and/or seasonally in oligotrophic regions of the
143 global ocean (Beckmann & Hense 2007; Mignot et al. 2014; Barbieux et al. 2019; Cornec et al.
144 2021). Considering the large (45%) surface areas covered by stratified oligotrophic regions in
145 the global ocean (McClain et al. 2004), improving the quantification of biological production
146 of organic carbon and characterizing the contribution of SCMs to the water-column production
147 in such regions are critical. For this purpose, *in situ* diel-resolved measurements with high
148 spatio-temporal resolution in the entire water column represent an intriguing opportunity of
149 vital importance.

150 In this study, we exploit summertime observations acquired by two BioGeoChemical-
151 Argo (BGC-Argo) profiling floats deployed in contrasted systems of the Mediterranean Sea.
152 This offers a unique opportunity for pursuing the exploration of the bio-optical diel cycle-based
153 approach to biological production in oligotrophic environments. One of the two BGC-Argo
154 floats was deployed in the Ligurian Sea in the vicinity of the BOUSSOLE fixed mooring

a supprimé: 4

a supprimé: the

a supprimé: of phytoplankton cells

a supprimé: to low light conditions

159 (BOUée pour l'acquiSition d'une Série Optique à Long termE; Antoine et al. 2008). This area
160 is representative of a seasonally stratified oligotrophic system, with a potentially productive
161 SCM (e.g. Mignot et al. 2014; Barbieux et al. 2019) that follows a recurrent spring bloom. The
162 second float was deployed in the Ionian Sea (Central Mediterranean) as part of the
163 PEACETIME (ProcEss studies at the Air-sEa Interface after dust deposition in the
164 MEditerranean sea) project (Guieu et al. 2020). The Ionian Sea is a nearly permanent
165 oligotrophic system (e.g. Lavigne et al. 2015) with an SCM induced mostly by
166 photoacclimation [of phytoplankton cells without concomitant increase of carbon biomass](#) (e.g.
167 Mignot et al. 2014; Barbieux et al. 2019).

168 The BGC-Argo profiling floats used in this study measured, among a suite of physical
169 and biogeochemical properties, the c_p and b_{bp} coefficients and were both programmed to sample
170 the entire water column at a high temporal resolution (4 vertical profiles per 24h), in order to
171 monitor the diel variations of the bio-optical properties. We applied, for the first time, a
172 modified version of the method of Claustre et al. (2008) to the diel c_p and b_{bp} measurements
173 acquired by the BGC-Argo floats to derive community production. Using this dataset, we (1)
174 assess the relevance of the diel cycle-based method for estimating biological production of
175 organic carbon in the considered regions and discuss the applicability of the method to b_{bp} , in
176 addition to c_p ; (2) investigate the regional and vertical variability of the production estimates
177 with a focus on the SCM layer in relation to the biological and abiotic context; (3) discuss the
178 relative contribution of the SCM layer to the water-column community production.

179 **2 Data and methods**

180 **2.1 Study region**

181 The Mediterranean Sea provides a unique environment for investigating the
182 biogeochemical functioning of oligotrophic systems that exhibit either a seasonal or permanent

183 SCM. The Mediterranean is a deep ocean basin characterized by a West-to-East gradient in
184 nutrients and chlorophyll *a* concentration (e.g. Dugdale & Wilkerson 1988; Bethoux et al. 1992;
185 Antoine et al. 1995; Bosc et al. 2004; D’Ortenzio & D’Alcalà 2009) associated with a deepening
186 of the SCM (Lavigne et al. 2012; Barbieux et al. 2019). The Ionian Sea in the eastern
187 Mediterranean is defined as permanently oligotrophic, with the SCM settled at depth over the
188 whole year. This system represents the oligotrophic end-member type of SCM (Barbieux et al.
189 2019), much like the subtropical South Pacific Ocean Gyre. By contrast, the Ligurian Sea in
190 the western Mediterranean is seasonally productive akin to a temperate system (e.g. Casotti et
191 al. 2003; Marty & Chiavérini 2010; Siokou-Frangou et al. 2010; Lavigne et al. 2015). The
192 mixed layer deepens significantly during the winter period, inducing seasonal renewal of
193 nutrients in the surface layer that supports the spring bloom (Marty et al. 2002; Lavigne et al.
194 2013; Pasqueron de Fommervault et al. 2015; Mayot et al. 2016). After the seasonal bloom, the
195 SBM intensifies throughout the summer and into early fall. This system represents the
196 temperate end-member type of SCM.

197 2.2 BGC-Argo multi-profiling floats and data processing

198 We deployed BGC-Argo floats programmed for “multi-profile” sampling in each of these
199 two regions (Fig. 1). The Ligurian Sea float (hereafter noted fLig, WMO: 6901776), was
200 deployed in the vicinity of the BOUSSOLE fixed mooring (7°54’E, 43°22’N) during one of the
201 monthly cruises of the BOUSSOLE program (Antoine et al. 2008) and profiled from April 9,
202 2014 to March 15, 2015. For the purpose of this study focusing on oligotrophic systems, we
203 selected the fLig float measurements acquired during the time period May 24 to September 13,
204 2014 to coincide in months with the Ionian Sea float time series. The Ionian Sea float (hereafter
205 noted fIon, WMO: 6902828) was deployed as part of the PEACETIME project (Guieu et al.
206 2020). We used the fIon float measurements acquired during the time period May 28 to

a supprimé: We deployed BGC-Argo floats programmed for “multi-profile” sampling in each of these two regions (Fig. 1). The Ligurian Sea float (hereafter noted fLig, WMO: 6901776), was deployed in the vicinity of the BOUSSOLE fixed mooring (7°54’E, 43°22’N) during one of the monthly cruises of the BOUSSOLE program (Antoine et al. 2008). We used the fLig float measurements acquired during the time period May 24 to September 13, 2014. The Ionian Sea float (hereafter noted fIon, WMO: 6902828) was deployed as part of the PEACETIME project (Guieu et al. 2020). We used the fIon float measurements acquired during the time period May 28 to September 11, 2017. Thus, although collected in different years, the data sets arise from similar seasonal contexts.

221 [September 11, 2017. Thus, although collected in different years, the data sets arise from similar](#)
222 [seasonal contexts.](#)

223 The BGC-Argo floats used in this study are “PROVOR CTS-4” (nke Instrumentation,
224 Inc.). They were both equipped with the following sensors and derived data products: (1) a
225 CTD sensor for depth, temperature and salinity; (2) a “remA” combo sensor that couples a
226 Saatlantic OCR-504 (for downwelling irradiance at three wavelengths in addition to
227 photosynthetic available radiation, PAR) and a WET Labs ECO Puck Triplet (for both
228 chlorophyll *a* (excitation/emission wavelengths of 470 nm/695 nm) and colored dissolved
229 organic matter (CDOM; 370 nm/460 nm) fluorescence, and particulate backscattering
230 coefficient at 700 nm); and (3) a WET Labs C-Rover (for particulate beam attenuation
231 coefficient at 660 nm, 25-cm pathlength). Data were collected along water column profiles from
232 1000 m up to the surface with a vertical resolution of 10 m between 1000 and 250 m, 1 m
233 between 250 and 10 m, and 0.2 m between 10 m and the surface. First, the BGC-Argo raw
234 counts were converted into geophysical units by applying factory calibration. Second, we
235 applied corrections following the BGC-Argo QC procedures (Schmechtig et al. 2015, 2016;
236 Organelli et al. 2017).

237 Factory-calibrated chlorophyll fluorescence requires additional corrections for
238 determining the chlorophyll *a* concentration (*Chl*). Values collected during daylight hours were
239 corrected for non-photochemical quenching following Xing et al. (2012). A global analysis of
240 factory-calibrated chlorophyll fluorescence measured with WET Labs ECO sensors relative to
241 concurrent chlorophyll *a* concentrations, determined by High Performance Liquid
242 Chromatography (HPLC), yielded a global overestimate bias of 2 (Roesler et al. 2017), with
243 statistically significant regional biases varying between 0.5 and 6. [The Mediterranean Sea is](#)
244 [known to show very small regional variations of the fluorescence-to-*Chl* ratio \(Taillandier et](#)
245 [al. 2018\), with a mean value close to 2 \(1.66±0.28 and 1.72±0.23 for the Western and Eastern](#)

a supprimé: A

a supprimé: In t

a supprimé: , the

a supprimé: are known to be very small

250 Mediterranean, respectively; Roesler et al. 2017). Hence the bias correction factor of 2 was
251 applied to BGC-Argo fluorescence data from both the Ligurian and Ionian regions, consistently
252 with the processing performed at the Coriolis Data Center.

253 For the particulate backscattering coefficient (b_{bp}), we followed the BGC-Argo
254 calibration and quality control procedure of Schmechtig et al. (2016). The backscattering
255 coefficient at 700 nm (m^{-1}) is retrieved following Eq. (1):

$$256 \quad b_{bp}(700) = 2 \pi \chi [(\beta b_{bp} - Darkb_{bp}) \times Scaleb_{bp} - \beta sw] \quad (1)$$

257 where $\chi = 1.076$ is the empirical weighting function that converts particulate volume
258 scattering function at 124° to total backscattering coefficient (Sullivan et al. 2013); βb_{bp} is the
259 raw observations from the backscattering meter (digital counts); $Darkb_{bp}$ (digital counts) and
260 $Scaleb_{bp}$ ($m^{-1} sr^{-1} count^{-1}$) are the calibration coefficients provided by the manufacturer; and
261 βsw is the contribution to the Volume Scattering Function (VSF) by the pure seawater at the
262 700 nm measurement wavelength that is a function of temperature and salinity (Zhang et al.
263 2009).

264 The calibration procedure applied to the particulate beam attenuation coefficient (c_p) is
265 similar to that described in Mignot et al. (2014). The beam transmission, T (%), is transformed
266 into the beam attenuation coefficient, c (m^{-1}), using the relationship:

$$267 \quad c = -\frac{1}{x} \ln \frac{T}{100} \quad (2)$$

268 where x is the transmissometer pathlength (25 cm). The beam attenuation coefficient c is the
269 sum of the absorption and scattering by seawater and its particulate and dissolved constituents.
270 At 660 nm, the contribution of CDOM (c_{CDOM}) can be considered negligible in oligotrophic
271 waters because, although its absorption in the blue is comparable to that of particulate material
272 (Organelli et al. 2014), the c_{CDOM} spectrum decays exponentially towards near zero in the red

a supprimé: ,

a supprimé: h

275 (Bricaud et al. 1981), and because it is comprised of dissolved molecules and colloids, its
276 scattering is negligible (Boss and Zaneveld 2003). Meanwhile $c_w(660)$ for pure water is constant
277 and removed in the application of the factory calibration; effects due to dissolved salt are
278 accounted for according to Zhang et al. (2009). Hence, at a wavelength of 660 nm, the particle
279 beam attenuation coefficient, c_p (m^{-1}), is retrieved by subtracting the seawater contribution to
280 c . The biofouling-induced signal increase that is observed in clear deep waters and results in a
281 drift in c_p values with time, is corrected as follows. For each profile, a median c_p value, used as
282 an “offset”, is computed from the c_p values acquired between 300 m and the maximum sampled
283 depth, and subtracted from the entire profile.

284 Using the solar noon Photosynthetically Available Radiation (PAR) measurements, we
285 computed the euphotic layer depth (Z_{eu}) as the depth at which the PAR is reduced to 1% of its
286 value just below the surface (Gordon & McCluney 1975) and the penetration depth (Z_{pd} ; also
287 known as the e-folding depth or first attenuation depth) as $Z_{eu} / 4.6$. We define the surface layer
288 from 0 m to Z_{pd} . We also define the SCM layer as in Barbieux et al. (2019), whereby a Gaussian
289 model is fit to each *Chl* vertical profile measured by the floats in order to determine the depth
290 interval of the full width half maximum of the SCM. Finally, the Mixed Layer Depth (MLD) is
291 derived from the float CTD data as the depth at which the potential density difference relative
292 to the surface reference value is 0.03 kg m^{-3} (de Boyer Montégut et al. 2004).

293 Unlike the majority of BGC-Argo floats that collect profile measurements every 10 days,
294 the two platforms used in this study sampled the water column with 4 profiles per day, albeit
295 with slightly different regimes (Fig. 2). The fLig float cycle commences with the first profile at
296 sunrise (t_{sr}), a second at solar noon (t_n), a third profile at sunset the same day (t_{ss}), and a fourth
297 profile at sunrise the next day (t_{sr+1}). The fLig float then acquires a profile at solar noon 4 days
298 later (t_{n+4}), and then restarts 3 days later the acquisition of 4 profiles in 24 hours from sunrise
299 (t_{sr+7}). The float cycle is performed over a single 24-hour period; it begins at sunrise (t_{sr}),

a supprimé: increasing

a supprimé: ing

a supprimé: second

a supprimé: third

a supprimé: ,

a supprimé: and a last one at solar noon the next day (t_{n+1}).
The sampling cycle is repeated every four days.

307 followed by a second profile at solar noon (t_n), a third at sunset (t_{ss}) and a last night profile at
308 approximately midnight (t_m). For this float, the sampling cycle is repeated each day.

309 2.3 Characterization of the diel cycle of the bio-optical properties

310 In order to characterize the amplitude and variability of the diel cycle of the c_p and b_{bp}
311 coefficients, we use the metrics defined by [Gernez et al. \(2011\)](#) and [Kheireddine & Antoine](#)
312 (2014). First, we compute the amplitude of the diurnal variation of the c_p and b_{bp} coefficients
313 as:

$$314 \Delta c_p = c_p(t_{ss}) - c_p(t_{sr}) \quad (3a)$$

$$315 \Delta b_{bp} = b_{bp}(t_{ss}) - b_{bp}(t_{sr}) \quad (3b)$$

316 with $c_p(t_{sr})$ and $b_{bp}(t_{sr})$ the values of c_p and b_{bp} at sunrise and $c_p(t_{ss})$ and $b_{bp}(t_{ss})$ the values at
317 sunset the same day.

318 We also consider the relative daily variation Δc_p and Δb_{bp} (expressed as % change) for
319 each float and each day of observation, from sunrise to sunrise as follows:

$$320 \Delta c_p = 100 \left(\frac{c_p(t_{sr})}{c_p(t_{sr+1})} - 1 \right) \quad (4a)$$

$$321 \Delta b_{bp} = 100 \left(\frac{b_{bp}(t_{sr})}{b_{bp}(t_{sr+1})} - 1 \right) \quad (4b)$$

322 with $c_p(t_{sr})$ and $b_{bp}(t_{sr})$ being the values of c_p and b_{bp} at sunrise and $c_p(t_{sr+1})$ and
323 $b_{bp}(t_{sr+1})$ the values at sunrise the next day. Then the mean and range in relative daily
324 variations ($\overline{m}\Delta$ and $\overline{r}\Delta$, respectively) are computed for each float over the entire time series.

325 2.4 Principle of the bio-optical diel cycle-based approach to biological production

326 The two bio-optical properties that we considered in this study, c_p and b_{bp} , are both
327 linearly correlated to, and thus may be used as a proxy for, the stock of POC (e.g. [Oubelkheir](#)
328 [et al. 2005](#); [Gardner et al. 2006](#); [Cetinić et al. 2012](#)). Both of these bio-optical proxies have been

a supprimé: W

a supprimé: (flon)

a supprimé: 3

a supprimé: Comparable computations for fLig were made from noon (t_n) to noon (t_{n+1}).

a supprimé: In this study we considered

a supprimé: distinct

a supprimé: i.e. the

a supprimé: coefficient ([Siegel et al. 1989](#); [Claustre et al. 2008](#)) ...

a supprimé: the

a supprimé: coefficient ([Barnes & Antoine 2014](#); [Kheireddine & Antoine 2014](#)). To first order, c_p and b_{bp}

342 shown to exhibit a diurnal cycle (e.g. Oubelkheir & Sciandra 2008; Loisel et al. 2011;
 343 Kheireddine & Antoine 2014). The daily solar cycle is a major driver of biological activity in
 344 all oceanic euphotic zones, which influences the abundance of microorganisms, including
 345 phytoplankton (Jacquet et al. 1998; Vaultot & Marie 1999; Brunet et al. 2007) and heterotrophic
 346 bacteria (Oubelkheir & Sciandra 2008; Claustre et al. 2008) and, therefore, the magnitude of
 347 the c_p and b_{bp} coefficients. Diel changes in the c_p or b_{bp} coefficient reflect processes that affect
 348 the cellular abundance (number) and the attenuation, or backscattering, cross-section, which
 349 varies with cell size and refractive index. The diurnal increase in c_p or b_{bp} has primarily been
 350 attributed to photosynthetic cellular organic carbon production (Siegel et al. 1998), that will
 351 first result in an increase in cell size, or an increase in cell abundance and a decrease in cell size
 352 following cell division often occurring at night. In addition, the diurnal increase in c_p or b_{bp} may
 353 be caused by variations in cellular shape and refractive index that accompany intracellular
 354 carbon accumulation (Stramski & Reynolds 1993; Durand & Olson 1996; Claustre et al. 2002;
 355 Durand et al. 2002). The nighttime decrease in c_p or b_{bp} may be explained by a decrease in
 356 cellular abundance due to aggregation, sinking or grazing (Cullen et al. 1992), a reduction in
 357 cell size and/or refractive index associated with cell division and respiration, the latter involving
 358 changes in intracellular carbon concentration with effect on the refractive index (Stramski &
 359 Reynolds 1993). Community composition and cell physiology (in response to diel fluctuations
 360 of the light field) might also influence the optical diel variability through their effects on cell
 361 size and refractive index. Diel variation in photoacclimation can be important in coastal
 362 communities dominated by microplankton (Litaker et al. 2002; Brunet et al. 2008).
 363 Nevertheless, previous studies conducted in oligotrophic environments suggest that
 364 photosynthetic growth is the major driver of the diurnal changes in c_p or b_{bp} (Gernez et al. 2002;
 365 Claustre et al. 2008). In addition, Claustre et al. (2002), in an experimental work based on
 366 *Prochlorococcus*, a frequent taxon in oligotrophic regions, show that although non-negligible,

a supprimé: ¶

a supprimé: (e.g. Oubelkheir & Sciandra 2008)

a supprimé: o first order, t

a supprimé: may

a supprimé: an increase in particle biomass

a supprimé: ing

a supprimé: from

a supprimé: particle abundance and/or

a supprimé: , both associated with

a supprimé: To second order, t

a supprimé:

a supprimé: particle

a supprimé: particle

a supprimé: particle

a supprimé: and

a supprimé: changes

a supprimé: particle

a supprimé: , or microorganism

a supprimé: .

a mis en forme : Police :Non Italique

386 the diel variability in photoacclimation is much less pronounced than that in phytoplankton
387 growth.

388 Following a modified version of Claustre et al. (2008), the observed daytime increase and
389 nighttime decrease in c_p -derived (or b_{bp} -derived) POC are used to estimate gross community
390 production. For this purpose, the c_p and b_{bp} coefficients, measured *in situ* by the BGC-Argo
391 profiling floats, are converted into POC equivalent using a constant c_p -to-POC (or b_{bp} -to-POC)
392 relationship from the literature (see below). By definition, the c_p and b_{bp} coefficients target
393 particles so that the dissolved biological matter is not accounted for by the present method.

394 2.5 Bio-optical properties-to-POC relationships

395 The conversion of c_p and b_{bp} into POC relies on the use of empirical proxy relationships
396 and assumptions concerning the variations in those relationships. First, as in Claustre et al.
397 (2008), we assume that the c_p - or b_{bp} -to-POC relationship remains constant on a daily timescale,
398 consistently with previous works (Stramski & Reynolds 1993; Cullen & Lewis 1995), so that
399 observed variations in the optical coefficients can be interpreted as variations in POC. Second,
400 the specific proxy value is not constant, as many empirical relationships between POC and c_p
401 (e.g. Claustre et al. 1999; Oubelkheir et al. 2005; Gardner et al. 2006; Loisel et al. 2011) or b_{bp}
402 (e.g. Stramski et al. 2008; Loisel et al. 2011; Cetinić et al. 2012) have been proposed for specific
403 regions (Tables 1 and 2). In the present study, we used the relationships from Oubelkheir et al.
404 (2005) and Loisel et al. (2011) for c_p and b_{bp} , respectively. Both relationships were established
405 from *in situ* measurements collected in the Mediterranean Sea and produce c_p - or b_{bp} -derived
406 POC values falling in the middle of the range of all the POC values resulting from the different
407 bio-optical relationships taken from the literature (Tables 1 and 2).

a supprimé: The bio-optical diel cycle-based approach used in this study relies on

a supprimé: . Following this approach

411 2.6 Estimating biological production from the diel cycle of POC

412 2.6.1 Hypotheses

413 The time-rate-of-change in depth-resolved POC biomass, $b(z,t)$, can be described by a
414 partial differential equation:

$$415 \frac{\partial b(z,t)}{\partial t} = \mu(z,t) b(z,t) - l(z,t) b(z,t), \quad (5)$$

416 where $\mu(z,t)$ is the particle photosynthetic growth rate and $l(z,t)$ the particle loss rate at depth
417 z and time t (both in units of d^{-1}). As in previous studies (Claustre et al. 2008, Gernez et al.
418 2011; Barnes and Antoine 2014), we assume a 1D framework. In other words, we ignore the
419 effects of lateral transport of particles by oceanic currents and assume that there is no vertical
420 transport of particles into or out of the layer considered. We also assume that the loss rate is
421 constant throughout the day and uniform with depth, i.e. $l(z,t) = l$. In this context, the time series
422 of profiles are first converted to depth-integrated biomass (from $b(z,t)$ to $B(t)$) for each of the
423 layers in question, and then integrated over time to determine daytime gain, nighttime loss, and
424 net daily production.

425 2.6.2 Calculation of the loss rate

426 During nighttime, there is no photosynthetic growth, so that Eq. (5) becomes:

$$427 \frac{\partial b(z,t)}{\partial t} = -l b(z,t). \quad (6)$$

428 The integration of Eq. (6) over depth yields an expression of the rate of change of the depth-
429 integrated POC biomass, $B(t)$:

$$430 \frac{\partial B(t)}{\partial t} = -l B(t), \quad (7)$$

431 with $B(t) = \int_{z_2}^{z_1} b(z,t) dz$, the POC integrated within a given layer of the water column,
432 comprised between the depths z_1 and z_2 (in $gC m^{-2}$). In this respect, we consider three different

a supprimé: quasi-

a supprimé: and

435 layers: the euphotic layer extending from $z_1 = 0$ m to $z_2 = Z_{eu}$; the surface layer extending from
 436 $z_1 = 0$ m to $z_2 = Z_{pd}$; and the SCM layer extending from $z_1 = Z_{SCM} - Z_{SCM,1/2}$ and $z_2 = Z_{SCM} +$
 437 $Z_{SCM,1/2}$, with Z_{SCM} the depth of the SCM and $Z_{SCM,1/2}$ the depth at which Chl is half of the SCM
 438 value.

439 Eq. (7) can be integrated over nighttime to obtain an equation for the loss rate l , as a
 440 function of the nocturnal variation of B :

$$441 \quad l = \frac{\ln\left(\frac{B_{SS}}{B_{SR+1}}\right)}{t_{SR+1} - t_{SS}}, \quad (8)$$

442 with $B(t_{SS})$ and $B(t_{SR+1})$ corresponding to the POC integrated within the layer of interest, at
 443 t_{SS} (sunset) and t_{SR+1} (sunrise of the next day).

444 2.6.3 Calculation of the production rate

445 The daily (24-hour) depth-integrated gross production of POC, P (in units of $\text{gC m}^{-2} \text{d}^{-1}$),
 446 is defined as:

$$447 \quad P = \int_{t_{SR}}^{t_{SR+1}} \int_{z_2}^{z_1} \mu(z, t) b(z, t) dz dt, \quad (9)$$

448 with t_{SR} the time of sunrise on day 1 and t_{SR+1} the time of sunrise the following day. Equation (5)
 449 can be used to express P as a function of l , $b(z, t)$, and the rate of change of $b(z, t)$:

$$450 \quad P = \int_{t_{SR}}^{t_{SR+1}} \int_{z_2}^{z_1} \left(\frac{\partial b(z, t)}{\partial t} + l b(z, t) \right) dz dt, \quad (10)$$

451 which yields:

$$452 \quad P = B_{t_{SR+1}} - B_{t_{SR}} + l \int_{t_{SR}}^{t_{SR+1}} B(t) dt. \quad (11)$$

453 where the gross production P is calculated as the sum of the net daily changes in POC biomass
 454 plus POC losses, assuming a constant rate (l) during daytime and nighttime.

455 Finally, using the trapezoidal rule, Eq. (11) simplifies into

a supprimé: and

a supprimé: particles

458
$$P = B_{t_{sr+1}} - B_{t_{sr}} + l \sum_{i=1}^j (t_{i+1} - t_i) \frac{B_{i+1} + B_i}{2}, \quad (12)$$

459 with l calculated from Eq. (8) and the index i corresponding to the different measurement time
 460 steps over the course of the diel cycle (t_{sr} , t_n , t_{ss} , and t_{sr+1} ; Fig. 2).

461 In [summary](#), Eq. (12) is applied to the time series of the BGC-Argo floats by using b_{bp}
 462 and c_p converted into POC equivalents, integrated within the euphotic, surface, and SCM layers
 463 to compute c_p - and b_{bp} -derived estimates of gross community production, P , in all three layers
 464 of the water column.

465 2.7 Primary production model

466 The community production estimates obtained from the bio-optical diel cycle-based
 467 method are evaluated against primary production values computed with the bio-optical primary
 468 production model of Morel (1991). Morel's model estimates the daily depth-resolved organic
 469 carbon concentration fixed by photosynthesis, using the noontime measurements of *Chl*,
 470 temperature and PAR within the water column by the BGC-Argo profiling floats as model
 471 inputs. The standard phytoplankton photophysiological parameterization is used for these
 472 calculations (Morel 1991; Morel et al. 1996).

473 2.8 Phytoplankton pigments and community composition

474 During the BOUSSOLE cruises conducted in 2014 (cruises #143 to #154) and the
 475 PEACETIME cruise, discrete seawater samples were taken at 10–12 depths within the water
 476 column from Niskin bottles mounted on a CTD-rosette system and then filtered under low
 477 vacuum onto Whatman GF/F filters (0.7- μ m nominal pore size, 25-mm diameter). The filters
 478 were flash-frozen in liquid nitrogen and stored at -80°C until analysis by HPLC following the
 479 protocol of Ras et al. (2008). The concentrations of phytoplankton pigments resulting from
 480 these analyses were used to estimate the composition of the phytoplankton assemblage. For this
 481 purpose, we used the diagnostic pigment-based approach (Claustre et al. 1994; Vidussi et al.

a supprimé: t_n , t_{ss} , t_{sr+1} , and t_{n+1} for the Ligurian Sea, and

a supprimé: m for the Ionian Sea

a supprimé: brief

485 2001; Uitz et al. 2006) with the coefficients of Di Cicco et al. (2017) to account for the
486 specificities of Mediterranean phytoplankton communities. This approach yields the relative
487 contribution to chlorophyll *a* biomass of major taxonomic groups merged into three size classes
488 (micro-, nano and picophytoplankton).

489 The fLig float was spatially distanced from the location of sampling at the BOUSSOLE
490 mooring site. Thus, it was necessary to identify the time shift for matching the cruise-sampled
491 analyses to the float profile measurements. This was achieved by performing a cross-correlation
492 analysis of the bio-optical time series measurements collected on the float with that on the
493 mooring (in this case *Chl*, *c_p* and *b_{bp}*). A positive time lag between the BOUSSOLE site and the
494 position of the fLig float during its drift is observed suggesting that the variations observed by
495 the float led that observed at BOUSSOLE by ~2 days. This small-time lag coupled with high
496 correlation coefficient values and long decorrelation time scales, indicate that the monthly
497 interpolated pigment data measured at the BOUSSOLE site may be considered as representative
498 of the pigment composition along the fLig float trajectory.

499 3 Results and discussion

500 We first provide an overview of the biogeochemical and bio-optical characteristics
501 measured by the two BGC-Argo profiling floats in the Ligurian and Ionian Seas. We then assess
502 the usefulness of the diel cycle of the *b_{bp}* coefficient for deriving community production, in
503 comparison to the *c_p*-derived estimates as a reference, and discuss the *c_p*-derived estimates.
504 Finally, we examine the community production estimates in both study regions, with an
505 emphasis on the SCM layer and its biogeochemical significance.

a supprimé: In this section, w

507 **3.1 Biogeochemical and bio-optical context in the study regions**

508 Both study regions are characterized by either seasonal or persistent oligotrophy, with
509 mean surface *Chl* values ranging within 0.08–0.22 mg m⁻³ (Fig. 3), and a stratified water column
510 with a consistently shallow MLD (<30 m). They do exhibit very different euphotic depths, with
511 a mean *Z_{eu}* of 47±5 m and 89±4 m in the Ligurian and Ionian Seas, respectively. Consistently,
512 the instantaneous midday PAR values are much lower in the upper layer of the Ligurian Sea
513 (93±70 μE m⁻² s⁻¹) than in the Ionian Sea (500±60 μE m⁻² s⁻¹) and shows a more rapid decrease
514 within the water column as phytoplankton biomass absorbs light. Both regions also display a
515 SCM, the depth of which co-occurs with *Z_{eu}* and the isopycnal 28.85 (i.e. the isoline of potential
516 density 28.85 kg m⁻³) over the considered time series, except for the last month of observation
517 in the Ionian Sea.

518 In the Ligurian Sea, the SCM is intense (1.06±0.34 mg Chl m⁻³; Fig. 3a), relatively
519 shallow (41±7 m), and associated with the subsurface *c_p* and *b_{bp}* maxima (0.27±0.09 and
520 0.0015±0.0006 m⁻¹, respectively; Fig. 3b–c). The *Chl* and *c_p* values are 5 times larger in the
521 SCM layer than at surface, and the *b_{bp}* values 3.6 times larger. In contrast, in the Ionian Sea,
522 the SCM is associated with lower values of *Chl* (0.27±0.07 mg m⁻³; Fig. 3d), *c_p* (0.05±0.01 m⁻¹;
523 Fig. 3e) and *b_{bp}* (0.0005±0.0001 m⁻¹; Fig. 3f). Compared to the Ligurian Sea SCM, the Ionian
524 Sea SCM is located twice as deep (97±11 m) and is uncoupled from the *c_p* and *b_{bp}* maxima that
525 occur at shallower depth.

526 Hence, the selected regions are representative of two contrasted SCM systems with
527 distinct degree of oligotrophy, consistent with our expectations (e.g. D’Ortenzio & Ribera
528 D’Alcalá 2009; Barbioux et al. 2019). Such a contrast in the SCM characteristics in relation
529 with the trophic gradient of the environment has already been observed in the Mediterranean
530 Sea (e.g. Lavigne et al. 2015; Barbioux et al. 2019) and on a global scale (e.g. Cullen 2015 and
531 references therein; Mignot et al. 2014; Cornec et al. 2021). These studies report that the depth

a supprimé: zon

a supprimé:

a supprimé: any

535 of the SCM is inversely correlated with the surface *Chl* (an index of the trophic status) and light
536 attenuation within the water column. Previous studies (Mignot et al. 2014; Barbieux et al. 2019;
537 Cornec et al. 2021) indicate that moderately oligotrophic, temperate conditions are generally
538 associated with a relatively shallow SCM coupled to a maximum in c_p or b_{bp} , reflecting an
539 increase in phytoplankton carbon biomass (SBM). In contrast, in the most oligotrophic
540 environments, the vertical distribution of *Chl* shows a maximum at greater depths and is
541 decoupled from the c_p or b_{bp} vertical distribution. Furthermore, Barbieux et al. (2019) show
542 that, in the northwestern Mediterranean region, the SCM mirrors a biomass maximum located
543 slightly above Z_{eu} , which benefits from an adequate light-nutrient regime thanks to a deep
544 winter convective mixing allowing nutrient replenishment in the upper ocean. In the Ionian Sea
545 where the MLD and nutricline are permanently decoupled, the SCM establishes below Z_{eu} as
546 phytoplankton organisms attempt to reach nutrient resources. Prevailing low-light conditions
547 lead to pronounced photoadaptation of phytoplankton. Thus, consistently with previous work,
548 the present observations indicate that the Ligurian Sea SCM is a phytoplankton carbon biomass
549 (SBM) likely resulting from favorable light and nutrient conditions, whereas the Ionian SCM
550 would be essentially induced by photoacclimation of phytoplankton cells.

551 Although the summer period is typically considered stable, some temporal variations are
552 observed over the time series that are more pronounced in the SCM layer than at surface. In the
553 Ligurian Sea SCM, the *Chl*, c_p and b_{bp} exhibit similar temporal evolution, with relatively high
554 values in late May 2014, followed by a marked decrease until mid-July (Figs. 4a–c). Then we
555 observe two local minima in *Chl*, c_p and b_{bp} that delineate a second peak between July 14 and
556 August 16, 2014 (as indicated by the dashed lines in Fig. 4a–c). In the Ionian Sea SCM, the
557 *Chl*, c_p and b_{bp} values all decrease from late May until a minimum is reached on August 11,
558 2017 (dashed line in Figs. 4d–e) and a second increase is recorded later in the season. These

a supprimé: These observations indeed

a supprimé: suggest

a supprimé: mirrors an increase in

a supprimé: is

a supprimé: †

564 temporal patterns are further discussed [in relation with the variability in the estimated POC and](#)
565 [production rates](#) (Section 3.4).

566 3.2 Assessment of the method

567 3.2.1 Analysis of the diel cycle of the c_p and b_{bp} coefficients

568 Diel cycles, characterized by a daytime increase and a nighttime decrease, are observed in
569 both c_p and b_{bp} time series in all layers of the water column, [as illustrated for the SCM layer of](#)
570 [the Ionian Sea in Fig. 5 \(examples of the diel cycles of \$c_p\$ and \$b_{bp}\$ for both the Ligurian and](#)
571 [Ionian Seas are provided in Appendix A\). Considering the time series of the Ligurian and Ionian](#)
572 [Seas, as well as the surface and SCM layers, the \$c_p\$ and \$b_{bp}\$ coefficients show mean diurnal](#)
573 [amplitudes, \$\Delta c_p\$ and \$\Delta b_{bp}\$, spanning between \$0.001 \text{ m}^{-1}\$ and \$0.02 \text{ m}^{-1}\$ and \$7 \times 10^{-6} \text{ m}^{-1}\$ and \$9 \times\$](#)
574 [10⁻⁵ \$\text{m}^{-1}\$, respectively. These results are consistent with Gernez et al. \(2011\), who observed \$\Delta c_p\$](#)
575 [values ranging within \$0.01 \text{ m}^{-1}\$ and \$0.07 \text{ m}^{-1}\$ in the surface layer of the Ligurian Sea](#)
576 [\(BOUSSOLE mooring\) during the summer to fall oligotrophic period. Relative to the mean \$c_p\$](#)
577 [and \$b_{bp}\$ values, the mean \$\Delta c_p\$ and \$\Delta b_{bp}\$ correspond to diurnal variations of 9–20% and 5–10%,](#)
578 [respectively.](#)

579 In the surface layer of the Ligurian Sea, the diel cycles of c_p and b_{bp} exhibit, respectively,
580 mean relative daily variation ($\overline{m\Delta}$) of 12.7% and 2.3%, and a range in relative daily variations
581 ($\overline{r\Delta}$) of 256.7% and 28.5% (Table 3). These values are of the same order of magnitude as those
582 reported by Kheireddine & Antoine (2014), acquired from the BOUSSOLE surface mooring in
583 the same area and during the oligotrophic season (from -5% to 25% for c_p and from -2% to 10%
584 for b_{bp}). Interestingly, the diel cycle of the c_p coefficient appears systematically more
585 pronounced than that of b_{bp} , with larger values of $\overline{m\Delta}$ and $\overline{r\Delta}$, regardless of the considered
586 region and layer of the water column (Table 3).

a supprimé: (

588 To first order, the variability in the b_{bp} and c_p coefficients is determined by the variability
589 in particle concentration, which underpins their robustness as POC proxies in open-ocean
590 conditions and explains their coherent evolution on a monthly timescale (Figs. 3–4).
591 Nevertheless, to second order, these coefficients vary differentially with the size and
592 composition of the particle pool. In particular, phytoplankton make a larger contribution to c_p
593 than b_{bp} , in part due to their strong absorption efficiency. In addition, b_{bp} is more sensitive to
594 smaller (<1 μm) particles (Stramski & Kiefer 1991; Ahn et al. 1992; Stramski et al. 2001; Boss
595 et al. 2004) and to particle shape and internal structure (Bernard et al. 2009; Neukermans et al.
596 2012; Moutier et al. 2017; Organelli et al. 2018). While the diel cycle of c_p would be essentially
597 driven by photosynthetic processes due to the influence of phytoplankton on c_p , b_{bp} would be
598 more responsive to detritus and/or heterotrophic bacteria that show minor, if not negligible,
599 daily variability. Hence, such specificities in the bio-optical coefficients may explain the
600 observed differences in their diel cycles.

601 Based on high-frequency surface measurements in the Ligurian Sea in various seasons, the
602 studies of Kheireddine & Antoine (2014) and Barnes & Antoine (2014) demonstrated that the
603 diel cycle of b_{bp} not only exhibits much reduced relative amplitude compared to that of c_p , but
604 the features of the b_{bp} cycle are not synchronous with that of the c_p cycle. Thus, b_{bp} cannot be
605 used interchangeably with c_p for assessing daily changes in POC or community production, but
606 perhaps provides additional information on the particulate matter and its production rates. Our
607 results support these previous findings, not only for the surface layer of the Ligurian Sea, but
608 also for the whole water column of both the Ligurian and Ionian regions.

609 We now consider the integrated euphotic zone gross community production estimates
610 derived from the bio-optical diel cycle-based method (Fig. 6). We compare the c_p - and b_{bp} -
611 based estimates with primary production estimates computed with the model of Morel (1991).
612 The b_{bp} -derived production rates underestimate those derived from c_p in both regions by about

a supprimé: t

a supprimé: than is c_p

615 a factor of ten, with respective mean values of $0.11 \pm 0.28 \text{ gC m}^{-2} \text{ d}^{-1}$ and $1.18 \pm 1.13 \text{ gC m}^{-2} \text{ d}^{-1}$
616 in the Ligurian Sea, and $0.04 \pm 0.04 \text{ gC m}^{-2} \text{ d}^{-1}$ and $0.46 \pm 0.11 \text{ gC m}^{-2} \text{ d}^{-1}$ in the Ionian Sea. In
617 addition, the b_{bp} -derived production is much lower than the primary production computed with
618 the model of Morel (1991), which has mean values of $0.91 \pm 0.14 \text{ gC m}^{-2} \text{ d}^{-1}$ in the Ligurian Sea
619 and $0.31 \pm 0.04 \text{ gC m}^{-2} \text{ d}^{-1}$ in the Ionian Sea. The significantly lower community production
620 rates are a direct effect of the dampened relative daily amplitude of the b_{bp} diel cycle (Table 3),
621 and the sensitivity of b_{bp} to the smaller heterotrophic and detrital particulate matter. The bio-
622 optical diel cycle-based method, whether applied to c_p or b_{bp} , yields an estimate of the
623 community production, i.e. that associated with the accumulation of phytoplankton *and* bacteria
624 biomass, which is necessarily larger than the primary (photo-autotrophic) production rates from
625 the Morel (1991) model. These questionable low values of community production, along with
626 the observation of a weak daily variability in b_{bp} , support the idea that the diel cycle of b_{bp} may
627 not be a reliable index for total community production rates, consistently with previous studies
628 (Kheireddine & Antoine 2014; Barnes & Antoine 2014). However, the utility of a b_{bp} -derived
629 community production may be revealed in elucidating rates for distinct size-based groups of
630 organisms, such as picoplankton. A better understanding of the specific size range that
631 dominates the diel cycle in b_{bp} will be important to understand. Yet, for our purposes, we
632 disregard the b_{bp} -based estimates and focus our analysis on the c_p -derived gross community
633 production estimates.

634 **3.2.2 Community production derived from the c_p coefficient**

635 The c_p -derived estimates of gross community production, integrated within the euphotic
636 layer, compare favorably with those found in the literature for similar Mediterranean areas (see
637 Table 4 and references therein). The c_p -based estimates show a 2.5-fold difference between the
638 Ligurian Sea and the Ionian Sea (mean of $1.18 \text{ gC m}^{-2} \text{ d}^{-1}$ and $0.46 \text{ gC m}^{-2} \text{ d}^{-1}$, respectively;
639 Table 6). In comparison, water column-integrated primary production values, either inferred

640 from satellite observations and biogeochemical models or measured *in situ*, vary within the
641 range 0.13–1 gC m⁻² d⁻¹ and 0.14–0.69 gC m⁻² d⁻¹ for the Western (or Ligurian) and Eastern (or
642 Ionian) region, respectively (Table 4). As expected, our c_p -based community production rates
643 are larger than published primary production rates. The present c_p -derived values also compare
644 favorably with gross community production estimates inferred from a similar approach applied
645 to bio-optical measurements from the BOUSSOLE mooring in the Ligurian Sea (0.5–0.8 gC m⁻²
646 d⁻¹ in Gernez et al. 2011; 0.8–1.5 gC m⁻² d⁻¹ in Barnes & Antoine 2014) and along an
647 oligotrophic gradient in the South Pacific Subtropical Ocean (0.85 gC m⁻² d⁻¹; Claustre et al.
648 2008).

649 The empirical relationships linking the c_p (or b_{pp}) coefficient to POC are known to exhibit
650 regional and seasonal variability in response to changes in the composition of the particle
651 assemblage and associated changes in particle size, shape and type, i.e. biogenic or mineral
652 (e.g. Stramski et al. 2004; Neukermans et al. 2012; Slade & Boss 2015). Hence, the choice of
653 such relationships strongly affects the conversion of the measured daily bio-optical variability
654 into POC fluxes. For the time period and study regions here, the c_p -based community
655 production varies by a factor of 2, depending on the selected bio-optical relationship, so that c_p -
656 based estimates vary between 0.89±0.84 gC m⁻² d⁻¹ and 1.62±1.54 gC m⁻² d⁻¹ in the Ligurian
657 Sea, and between 0.35±0.09 gC m⁻² d⁻¹ and 0.63±0.16 gC m⁻² d⁻¹ in the Ionian Sea. The minimal
658 and maximal values are obtained with the bio-optical relationships from Marra et al. (1995) and
659 Stramski et al. (2008), respectively (Table 5). Compared to the reference value obtained using
660 the Oubelkheir et al. (2005) relationship, the c_p -based estimates are 25% lower and 37% higher
661 using the relationships of Marra et al. (1995) and Stramski et al. (2008), respectively. We also
662 note that using the Mediterranean relationship of Loisel et al. (2011), instead of that of
663 Oubelkheir et al. (2005), would reduce the c_p -based estimates by 17% in both study regions

a supprimé: in May–August;

665 [\(Table 5\). That said, although the absolute magnitudes vary depending upon proxy choice, the](#)
666 [differences observed between locations is robust.](#)

667 The use of the single relationship established from Mediterranean waters (Oubelkheir et al.
668 2005) appears as a reasonable choice for the study region. Yet, if more relevant bio-optical
669 proxy relationships are available, such as one that accounts for spatial and seasonal variations,
670 and even applicable to different layers of the water column, that would certainly reduce the
671 uncertainty in the rate estimation. Although this is beyond the scope of the present study, we
672 recognize that such investigations should be conducted in the future in order to refine optics-
673 based biomass (POC) and community production estimates.

674 3.3 Regional and vertical variability of production

675 The temporal evolution of the c_p -derived POC biomass integrated within the three distinct
676 layers of the water column is presented for the two study regions in Fig. 7. The integrated POC
677 concentration values follow similar temporal trends as reported for c_p (Figs. 3–4). In the
678 Ligurian Sea, the euphotic layer-integrated POC varies between 1.5 and 6.0 gC m⁻² (mean of
679 3.7±1.1 gC m⁻²; Fig. 7a and Table 6). There was a decrease from late May to mid-July (6.0 to
680 1.5 gC m⁻²) followed by a moderate peak (3.9 gC m⁻²) between mid-July and mid-August (as
681 bounded by the dashed lines in Fig. 5). The c_p -based community production did exhibit large
682 variability over the time period (Fig. 7b and Table 6), but interestingly, the moderate POC peak
683 observed in the core of the oligotrophic season (between mid-July and mid-August) is
684 associated with the maximum production rate of the time series (4.3 gC m⁻² d⁻¹).

685 In the Ionian Sea, the POC biomass integrated within the euphotic zone is much lower
686 than in the Ligurian Sea and remains more stable over the time period (1.9±0.24 gC m⁻²; Fig.
687 7c and Table 6). As with POC, the community production is much lower in the Ionian Sea than
688 in the Ligurian Sea, but still exhibits substantial variability with values ranging within 0.06–

689 0.68 gC m⁻² d⁻¹ (Fig. 7d). These results are consistent with multiple studies reporting a large
690 difference in the trophic status and productivity of the Ligurian and Ionian Seas, on seasonal
691 and annual timescales (D’Ortenzio & Ribera d’Alcala, 2009; Siokou-Frangou et al. 2010;
692 Lavigne et al. 2013; Mayot et al. 2016). Our results confirm this difference, yet on a monthly
693 timescale during the oligotrophic summer period.

694 The gross community production estimates integrated over different layers of the water
695 column reveal distinct patterns. In the Ligurian Sea, both the euphotic and SCM layers show
696 large production rates (0.96±1.3 gC m⁻² d⁻¹), with production in the SCM layer frequently
697 equaling or overtaking on the production in the euphotic layer (Fig. 7b). This is particularly
698 striking in late July, when the production peak is actually associated with a large enhancement
699 of the production in the SCM layer (4.9 gC m⁻² d⁻¹). In contrast, the surface layer shows reduced
700 production rates (0.29±0.33 gC m⁻² d⁻¹), a pattern also observed in the Ionian Sea (0.11±0.04
701 gC m⁻² d⁻¹). In the Ionian Sea, the production is maximal in the euphotic zone, and very variable
702 and occasionally larger in the SCM layer (0.14±0.39 gC m⁻² d⁻¹; Fig. 7d). The bio-optical diel
703 cycle-based method produces several occurrences of negative values in the SCM layer,
704 indicating that the $\downarrow D$ assumption is occasionally not satisfied in the lower part of the euphotic
705 layer. This could arise when physical processes that transport particles are larger than local
706 growth and loss of POC.

707 Our results support the hypothesis raised in previous studies (e.g. Mignot et al. 2014;
708 Barbieux et al. 2019) that, in the Ligurian temperate-like system, the SCM, which is in fact a
709 SBM, may be highly productive. Conversely, in the Ionian region, which shows similarities
710 with subtropical stratified oligotrophic systems, the SCM primarily reflects photoacclimation
711 and is less productive. Beyond these mean regional trends, both SCM systems exhibit some
712 temporal variability in production, a somewhat unexpected pattern at the core of the presumably
713 stable oligotrophic season.

a supprimé: quasi-

a supprimé: -

a supprimé: n

717 **3.4 Production in the SCM layer in relation with the biotic and abiotic context**

718 Here we investigate the temporal variability in the SCM layer production and attempt to
719 interpret the observed patterns in the context of biological and abiotic conditions.

720 **3.4.1 Phytoplankton and particulate assemblage**

721 The pigment data collected during the BOUSSOLE and PEACETIME cruises
722 concomitantly with the deployments of the fLig and fIon floats, respectively, are used as proxies
723 for phytoplankton community structure (Fig. 8). In the Ligurian Sea, nanophytoplankton
724 (mainly prymnesiophytes) appear as dominant contributors to the phytoplankton assemblage
725 both in the surface layer ($48\pm 8\%$; Fig. 8b) and SCM layer ($54\pm 10\%$). Picophytoplankton
726 (prokaryotes and small chlorophytes) and microphytoplankton (diatoms and dinoflagellates)
727 are present in moderate proportions, with $30\pm 11\%$ and $22\pm 5\%$ in the upper layer, and $19\pm 7\%$
728 and $27\pm 9\%$ in the SCM layer, respectively (Figs. 8a and 8c). No marked shift in the community
729 composition is observed during the timeseries, although occasional increase in the contribution
730 of microphytoplankton is observed in the SCM layer, with no clear temporal trend (Fig. 8a and
731 Appendix B). In the Ionian Sea, the surface layer displays large contribution of
732 nanophytoplankton ($56\pm 2\%$; Fig. 8e) and, to a lesser extent, picophytoplankton ($29\pm 3\%$; Fig.
733 8d). However, the SCM level is characterized by an enhanced contribution of
734 microphytoplankton (diatoms) to the algal assemblage ($49\pm 5\%$; Fig. 8f), as discussed in
735 Marañón et al. (2021). The Ionian PEACETIME data was limited to the period from May 25 to
736 28, 2017, and thus it was not possible to determine whether the composition of phytoplankton
737 communities evolved with time. Although not characterized by the prokaryotic populations
738 (*Synechococcus* and *Prochlorococcus*) that typically prevail in stratified oligotrophic
739 environments, our observations are consistent with previous studies reporting enhanced
740 contributions of nanophytoplankton (e.g. Gitelson et al. 1996; Vidussi et al. 2001) and the

a supprimé: change

a supprimé: .

743 occurrence of diatoms at depth (Siokou-Frangou et al. 2010; Crombet et al. 2011; Marañón et
744 al. 2021) in the Mediterranean Sea.

745 Bio-optical properties and their ratios provide indication about variations in the constituents
746 (algal or nonalgal) and size of the particulate pool, the composition of the phytoplankton
747 assemblage and the physiological status of phytoplankton cells (e.g. Geider 1987; Ulloa et al.
748 1994; Stramski et al. 2004; Loisel et al. 2007). Here we consider the bio-optical ratios b_{bp} / c_p ,
749 c_p / Chl , and b_{bp} / Chl in the SCM layer (Fig. 9). The b_{bp} / c_p ratio, while at slightly different
750 wavelengths (700 nm and 660 nm, respectively) are at absorption minima and thus this ratio is
751 comparable to the backscattering ratio b_{bp} / b_p . The b_{bp} / b_p ratio is a demonstrated proxy for
752 determining relative constituent composition (Twardowski et al. 2001), with phytoplankton
753 exhibiting lower ratios than nonalgal particles (approximately 0.5% and 1%, respectively; Boss
754 et al. 2004; Whitmire et al. 2007; Westberry et al. 2010). The b_{bp} / Chl and c_p / Chl ratios are
755 both proxies for the POC / Chl ratio (e.g. Claustre et al. 1999; Oubelkheir et al. 2005;
756 Behrenfeld et al. 2015; Álvarez et al. 2016), and thus an indicator of the contribution of
757 phytoplankton to the whole organic carbon pool. The variations are also interpreted as changes
758 in the composition of phytoplankton communities (e.g. Sathyendranath et al. 2009) and their
759 acclimation to the light-nutrient regime (e.g. Geider et al. 1987; Loisel & Morel 1998; Geider
760 et al. 1997; Cloern 1999) if one assumes that nonalgal particles are negligible (e.g., as indicated
761 by the backscattering ratio) or not varying in concentration. The differences between the $b_{bp} /$
762 Chl and c_p / Chl ratios lie in the fact that they are sensitive to different particle size ranges
763 (Roesler and Boss 2008) and, thus, when they are not correlated, one can qualitatively discern
764 differing dynamics across the phytoplankton size spectrum.

765 The b_{bp} / c_p ratio is very different between the Ligurian and Ionian Seas, with significantly
766 lower values in the Ligurian Sea (0.0068 ± 0.0009 and 0.0095 ± 0.0009 ; Fig. 9). These ratios
767 indicate that, in the general sense, the Ligurian Sea SCM is more phytoplankton dominated than

a supprimé: or $0.68 \pm 0.09\%$

a supprimé: or $0.95 \pm 0.09\%$

770 the Ionian Sea SCM, which tends towards nonalgal particles. In the Ligurian Sea, the b_{bp} / c_p
771 ratio remains <0.0087 and reaches a minimum of 0.0055 over the period coinciding with the
772 production event from mid-July to mid-August (Fig. 9a), consistent with phytoplankton
773 dominance. In contrast, in the Ionian Sea SCM, the b_{bp} / c_p ratio increases from 0.0085 in late
774 May, peaking at nearly 0.012 in early August, and then decreasing back to 0.0085 in September
775 (Fig. 9b). The tendency towards a ratio of 0.01 (or 1%) in the core of the oligotrophic season,
776 evidences the increased proportion of nonalgal particles to the bulk pool as previously observed
777 in oligotrophic environments (Yentsch & Phinney 1989; Stramski et al. 2004; Loisel et al.
778 2007).

779 The c_p and b_{bp} to Chl ratios exhibit not only different temporal patterns between the Ligurian
780 and Ionian Sea SCMs, they also exhibit different relative values. The c_p / Chl ratio in the
781 Ligurian Sea SCM is higher than that of the Ionian Sea, ranging from 0.18 to $0.45 \text{ m}^2 \text{ mg Chl}^{-1}$
782 ¹ (mean value of $0.29 \pm 0.06 \text{ m}^2 \text{ mg Chl}^{-1}$), compared to 0.15 to $0.26 \text{ m}^2 \text{ mg Chl}^{-1}$ (mean value
783 of $0.20 \pm 0.03 \text{ m}^2 \text{ mg Chl}^{-1}$), respectively. These results are consistent with the study of Loisel
784 & Morel (1998), reporting low values ranging within $0.1\text{--}0.2 \text{ m}^2 \text{ mg Chl}^{-1}$ at the deep
785 chlorophyll maximum level of oligotrophic sites. In contrast, although the b_{bp} / Chl ratio in the
786 Ligurian Sea SCM ranges from 0.0011 to $0.0023 \text{ m}^2 \text{ mg Chl}^{-1}$, and the Ionian Sea from 0.0015
787 to $0.0021 \text{ m}^2 \text{ mg Chl}^{-1}$, they have essentially identical mean values over the time series
788 (0.0017 ± 0.0006 and 0.0017 ± 0.0001 , respectively). The b_{bp} / Chl ratio being more sensitive to
789 small-sized particles than the c_p / Chl ratio, these results suggest that, in the SCM layer, the
790 POC in the small size fractions of the Ligurian and Ionian Seas is more similar than that in the
791 large size fractions.

792 Temporally, the Ligurian Sea SCM exhibits significantly more temporal variations in both
793 ratios compared to the Ionian Sea SCM, and the temporal variations are highly correlated. Both
794 the c_p / Chl and b_{bp} / Chl ratios in the Ligurian Sea SCM exhibit a peak at the start of the time

a supprimé: (0.87%)

a supprimé: (0.55%)

a supprimé: (0.85%)

a supprimé: (1.2%)

a supprimé: (0.85%)

a supprimé: .

a supprimé: This suggests that the POC in the smaller size fractions are more similar in their respective SCM than in their larger size fractions

804 series in late May that decreases to mid-July, followed by a second peak during the period
805 coinciding with the production episode from mid-July to mid-August, and then a third increase
806 until the end of the time series (Figs. 9b–c). In contrast, both ratios in the Ionian Sea SCM
807 exhibit significantly reduced temporal variability (Figs. 9e–f), with a weak increase is observed
808 starting in early August.

809 Despite differing temporal variability, the b_{bp} / Chl ratio in both Seas remains moderate to
810 low ($<0.0025 \text{ m}^2 \text{ mg Chl}^{-1}$; Figs. 9c and 9f), consistent with global SCM values (Barbieux et
811 al., 2018). The enhanced b_{bp} / Chl values observed in the Ligurian Sea SCM in early May, late
812 July and late August suggest an increased contribution of small (pico- and nano-sized)
813 phytoplankton (Cetinić et al. 2012; Cetinić et al. 2015). Yet, the BOUSSOLE pigment data do
814 not reveal pronounced changes in the phytoplankton assemblage. Low-light conditions
815 typically prevailing in the SCM layer are usually associated with low values of the c_p / Chl and
816 b_{bp} / Chl ratios (e.g. Loisel & Morel 1998; Behrenfeld & Boss 2003; Westberry et al., 2008;
817 Barbieux et al. 2019). These low values may reflect photoacclimation, by which phytoplankton
818 organisms increase their intracellular Chl , and/or an increase in the fluorescence-to- Chl ratio in
819 relation to limited or null non-photochemical chlorophyll fluorescence quenching.
820 Nevertheless, the temporal variability in the c_p / Chl and b_{bp} / Chl values may be resulting from
821 fluctuations in the light conditions at the SCM in the Ligurian Sea. In the Ionian Sea, the
822 invariant low c_p / Chl and b_{bp} / Chl values are consistent with both photoacclimation of
823 phytoplankton to low-light conditions and a diatom-dominated phytoplankton assemblage
824 (Cetinić et al. 2015; Barbieux et al. 2018). The relatively stable ratios observed in this region
825 suggest a relative steadiness in the composition of the phytoplankton assemblage over the
826 considered period.

a supprimé: (

a supprimé: ,

a supprimé: caused by

a supprimé: .

831 **3.4.2 Relation to abiotic conditions**

832 The Ligurian Sea exhibits enhanced community production during the period from mid-
833 July to mid-August 2014, which is associated with a comparatively moderate increase in the
834 biomass indicators (Figs. 3–4) and c_p -derived POC (Fig. 7a). During this time period, the depth
835 of the SCM shoals by 25 m. This change occurs concurrently with a slight shoaling of the
836 density isopycnals (Figs. 3a–c), and a doubling (from 0.5 to 1 mol quanta $m^{-2} d^{-1}$) in the daily
837 PAR within the SCM layer (Fig. 10a). Therefore, we suggest that the observed production
838 episode may result from physical forcing that induces an upwelling of the water mass, thereby
839 resulting in an alleviation of the light/nutrient limitation and an adequate balance between light
840 and nutrient availability in the SCM layer. This SCM production episode is associated with a
841 moderate phytoplankton biomass ($0.8 \text{ Chl } mg \text{ } m^{-3}$), dominated by a nanoplankton community.
842 It coincides with an increase in the c_p / Chl and b_{bp} / Chl ratios, which we attribute to a boost in
843 the carbon-to-*Chl* ratio resulting from production in enhanced light conditions. Because it
844 appears to result from changes in light conditions, we may attribute this production event to
845 photosynthetic (not community) growth.

a supprimé: phytoplankton

846 In the Ionian Sea, the depth of the SCM follows the depth of the isopycnal 28.85 during
847 the period from late to May to mid-August 2017 (Figs. 3d–f). In mid-August, the SCM reaches
848 its deepest point (~125 m) concurrent with deepening isopycnals, decreased PAR levels within
849 the SCM layer (Fig. 10b) and minimum values of *Chl*, c_p and b_{bp} . Afterwards, the SCM depth
850 decouples from the position of the isopycnals (Fig. 3d–f), the SCM becomes shallower and the
851 mean daily PAR in the SCM layer increases. Nevertheless, the observed temporal fluctuations
852 in the abiotic forcing and biological indicators do not seem to relate with any clear change in
853 the community production (Figs. 7d–f). This suggests that physics-induced changes in the
854 position of the SCM are not sufficient to alleviate the light and/or nutrient limitation occurring
855 at this time in the study location (Guieu et al. 2020). Considering the large contribution of

a supprimé: considered

a supprimé: area

859 diatoms at the SCM, one may conclude that the low, yet non-negligible, production levels
860 estimated in the SCM layer are supported by diatoms. This result supports previous findings
861 that indicate, contrary to the classic view of diatoms thriving essentially in dynamic eutrophic
862 conditions, these organisms have the ability to maintain in stratified oligotrophic environments,
863 including in deep layers under low light-nutrient conditions (Kemp & Villareal 2013; Kemp &
864 Villareal, 2018). This was also highlighted by Marañón et al. (2021) based on observations in
865 the Mediterranean Sea (PEACETIME cruise).

a supprimé: ing

a supprimé: that

866 3.5 Contribution of the SCM to the water column production

867 In order to assess the relative contribution of the SCM layer to the production occurring
868 in the whole water column, we compare the c_p -based estimates integrated within the productive
869 layer (0–1.5 Z_{eu}) and SCM layers. Our results suggest that, for these oligotrophic systems, the
870 production integrated within the SCM layer represents a substantial fraction (F_{SCM}) of the gross
871 community production integrated within the productive layer. This is particularly the case for
872 the Ligurian Sea where F_{SCM} reaches ~42%, and to a lesser extent for the Ionian Sea with F_{SCM}
873 ~16%.

874 Subtropical stratified oligotrophic gyres cover 45% of the global ocean (McClain et al.
875 2004). Assuming that the Ionian Sea is representative of such systems (e.g. Mignot et al. 2014;
876 Barbieux et al. 2019), and extrapolating the estimated relative contribution of the SCM layer to
877 the water column production in the Ionian (F_{SCM} ~16%), then the SCM layer would contribute
878 ~7% of the community production of the water column on a global scale (i.e. F_{SCM} of 16%
879 multiplied by a global spatial occurrence of 45%). In addition, using a global BGC-Argo
880 database, Cornec et al. (2021) estimated that SCMs in oligotrophic subtropical gyres behave as
881 SBM 8–42% of the year, depending on the season. Thus, assuming the Ligurian SCM
882 oligotrophic summer system as a reference for SBM, the contribution of the SCM layer to the

885 global water column production could seasonally reach 19% (i.e. F_{SCM} of 42% multiplied by a
886 global spatial occurrence of 45%).

887 We recognize that these estimates are very crude and need to be refined and confirmed in
888 future studies. Yet they suggest that the contribution of the SCM layer to the water column
889 production may be significant globally, although commonly ignored. Our observations are
890 consistent with previous findings [in the Mediterranean Sea](#) (Crombet et al. 2011; [Marañón et](#)
891 [al. 2021](#)) and [in other regions of the world ocean](#) (Kemp & Villareal 2013; Mignot et al. 2014),
892 and suggest that stratified oligotrophic systems should no longer be considered as steady
893 oceanic deserts and that their biogeochemical contribution should be accounted for and better
894 quantified to improve global carbon budgets.

895 4 Conclusions

896 The present study represents a first attempt to apply the bio-optical diel cycle-based
897 method (Siegel et al. 1989; Claustre et al. 2008) to the c_p and b_{bp} coefficients measured by two
898 BGC-Argo profiling floats. It aims to quantify gross community production in different layers
899 of the water column, the subsurface chlorophyll maximum (SCM) layer in particular, during
900 the oligotrophic summer season in two distinct systems of the Mediterranean, i.e. the Ligurian
901 Sea and the Ionian Sea.

902 From a methodological point of view, our results indicate that, compared to the c_p
903 coefficient, the diel cycle of the b_{bp} coefficient is not an optimal proxy for the daily POC
904 variations [regardless of the water column layer and \(Ligurian or Ionian\) region under](#)
905 [consideration](#). These results have major implications for use of the methodology with
906 geostationary ocean color missions and standard BGC-Argo profiling floats that yield only the
907 b_{bp} coefficient. The present results thus argue in favor of a frequent implementation onto BGC-
908 Argo floats of transmissometers (c_p sensors), which provide information on a suite of key

a supprimé: , so that we are not confident using the b_{bp} -based gross community production estimates, although it may provide a more robust proxy for the fraction of particulate matter in the smaller size classes

a supprimé: Our results for the surface layer of the Ligurian Sea are consistent with previous studies from moored observations (Kheireddine & Antoine 2014; Barnes & Antoine 2014), and we found they are valid for the entire water column and for both the Ligurian and Ionian Seas.

918 biogeochemical variables (Claustre et al. 2020), from phytoplankton community composition
919 (Rembauville et al. 2017), to particle flux export (Briggs et al. 2011; Estapa et al. 2013) and, as
920 demonstrated here, biological production (White et al. 2017; Briggs et al. 2018).

921 Our c_p -based gross community production rates compare consistently with previous
922 estimates from a similar approach applied to oligotrophic waters (Claustre et al. 2008; Gernez
923 et al. 2011; Barnes & Antoine 2014). Nevertheless, these estimates on average decrease by 25%
924 or increase by 37% depending on the used c_p -to-POC relationship, which is not negligible and
925 raises the question of the selection of an empirical bio-optical relationship for converting c_p into
926 POC equivalent. Hence, we recommend POC sampling simultaneously to BGC-Argo floats
927 deployment. This will help to better constrain bio-optical relationships and ultimately improve
928 the reliability of the biomass and production estimates.

929 Our results indicate that both the Ligurian and Ionian Seas may sustain relatively large
930 levels of gross community production during the oligotrophic summer period, with a substantial
931 contribution by the SCM layer, a feature characteristic of oligotrophic systems that is typically
932 considered as steady and non-productive. Our results also suggest that the contribution of the
933 SCM layer varies broadly depending the considered system, whether seasonally (Ligurian Sea)
934 or permanently (Ionian) oligotrophic. These results agree with previous BGC-Argo-based
935 studies describing the occurrence and functioning of SCM systems in the global ocean (Mignot
936 et al. 2014; Cornec et al. 2021) and Mediterranean Sea (Lavigne et al. 2015; Barbioux et al.
937 2019), and offer a first attempt to quantify biological production in such systems.

938 Our study emphasizes the promising potential of BGC-Argo profiling floats for providing
939 a non-intrusive, high-frequency assessment of POC production within the whole water column,
940 which is critical in particular for applications to stratified oligotrophic environments with
941 recurring or permanent SCMs. The present results, based on data from two Mediterranean
942 environments, should be confirmed in the future through the deployment of “multi-profiling”

a supprimé: These values are also consistent with estimates of primary production either computed from the model of Morel (1991) coupled to the considered BGC-Argo data, or published in the literature, although admittedly higher. This is unsurprising because the present estimates are based on the c_p coefficient, which accounts for both autotrophic and heterotrophic organisms (not just phytoplankton). This nevertheless raises the question of the selection of an empirical bio-optical relationship, which is key to converting c_p into POC equivalent. In the present study

a supprimé: c_p -derived production

a supprimé: bio-optical

a supprimé: In the Ligurian, the SCM behaves as a subsurface biomass maximum (SBM) and appears to respond to episodic abiotic forcing, with increased production rates coinciding with enhanced light availability in response to shoaling isopycnals and SCM. In this system, the particle assemblage is dominated by phytoplankton organisms, mainly nanoflagellates. In contrast, the Ionian SCM layer essentially reflects photoacclimation of phytoplankton cells to prevailing environmental conditions. It does not seem affected by modifications in abiotic forcing, although the phytoplankton assemblage appears to be dominated by diatoms.

a supprimé: More generally, our study suggests that the contribution of the SCM layer to the water column production varies broadly depending the considered system, whether seasonally (~42% in the Ligurian Sea) or permanently (~16% in the Ionian Sea) oligotrophic.

972 BGC-Argo floats in the broad, remote subtropical gyres. In such systems, biological production
973 is not constant but, instead, shows high temporal heterogeneity (Karl et al. 2003; Claustre et al.
974 2008) that may be missed by traditional sampling, leading to a potential underestimate of the
975 biogeochemical impact of these systems in global carbon budgets. Implementing such a BGC-
976 Argo-based approach to carbon flux quantification becomes even more important in the
977 perspective of climate change, which is predicted to induce an expansion of stratified
978 oligotrophic gyres and an oligotrophication of the oceans (Sarmiento et al. 2004) as already
979 observed from satellite imagery (Polovina et al. 2008; Signorini et al. 2015).

980

981 *Author contribution* MB, JU and AB designed the work and prepared the manuscript. MB
982 processed the data and conducted the analyses. MB, JU and CR prepared the plots. AM and BG
983 developed the biological production model. AM helped with the implementation of the model
984 and the interpretation of the output data. CR contributed to the analysis of the diel bio-optical
985 variability, interpretation of bio-optical data and the organization of the manuscript. HC
986 contributed to the interpretation of the BGC-Argo data and biological production. HL helped
987 with the interpretation of the bio-optical data and the global extrapolation of the results. VT and
988 FDO contributed to the BGC-Argo float deployments and interpretation of the physical data.
989 AP prepared and tested the BGC-Argo floats prior to deployment and set up the raw data stream.
990 EL and CP developed the BGC-Argo float version used in this study and contributed to float
991 preparation. CS handled BGC-Argo data archiving and distribution. All authors reviewed and
992 approved the manuscript.

993

994 *Data availability* The BGC-Argo profiling float data and metadata used in this paper may
995 be downloaded from the Argo GDAC (<http://doi.org/10.17882/42182>). All other original data
996 are available from the Argo Global Data Assembly Center (<ftp://ftp.ifremer.fr/ifremer/argo>).

997 These data were collected and made freely available by the International Argo Program and the
998 national programs that contribute to it (<http://www.argo.ucsd.edu>; <https://www.ocean-ops.org>).
999 The Argo Program is part of the Global Ocean Observing System. The PEACETIME project
1000 pigment data are available from the SEANOE archive under the following reference: Guieu et
1001 al., Biogeochemical dataset collected during the PEACETIME cruise, SEANOE,
1002 <https://doi.org/10.17882/75747>, 2020. The BOUSSOLE program pigment data may be
1003 accessed upon request (http://www.obs-vlfr.fr/Boussole/html/boussole_data/login_form.php).
1004

1005 *Acknowledgement* This paper represents a contribution to the following projects:
1006 PEACETIME (<https://doi.org/10.17600/17000300>), a joint initiative of the MERMEX and
1007 ChArMEx components supported by CNRS-INSU, IFREMER, CEA, and Météo-France as part
1008 of the program MISTRALS coordinated by INSU; PEACETIME-OC supported by the French
1009 program CNES-TOSCA; remOcean funded by ERC (grant 246777); and NAOS funded by
1010 ANR Equipex (grant J11R107-F). MB was funded by a PhD grant from Sorbonne Université
1011 (Ecole Doctorale 129). Phytoplankton pigment analyses were performed at the SAPIGH
1012 national HPLC analytical service at the Institut de la Mer de Villefranche (IMEV). We
1013 acknowledge the captains and crew of the Téthys and Pourquoi Pas? research vessels during
1014 the BOUSSOLE and PEACETIME cruises, as well as David Antoine, PI of the BOUSSOLE
1015 project, and Cécile Guieu and Karine Desboeufs, PIs of the PEACETIME project. We thank
1016 the International Argo Program and Coriolis project, which contributed to making the data
1017 freely and publicly available. Marin Cornec is also warmly thanked for useful discussion
1018 regarding biological production in SCM systems. [We finally wish to thank the two anonymous](#)
1019 [Reviewers and the co-Editor-in-Chief for their useful comments and suggestions.](#)
1020

1021 **References**

- 1022 Ahn, Y.-H., Bricaud, A., and Morel, A.: Light backscattering efficiency and related properties
1023 of some phytoplankters, *Deep-Sea Res. Pt. A*, 39, 1835–1855,
1024 [https://doi.org/10.1016/0198-0149\(92\)90002-B](https://doi.org/10.1016/0198-0149(92)90002-B), 1992.
- 1025 Allen, J.I., Somerfield, P.J., and Siddorn, J.: Primary and bacterial production in the
1026 Mediterranean Sea: a modelling study, *J. Mar. Syst.*, 33–34, 473–495,
1027 [https://doi.org/10.1016/S0924-7963\(02\)00072-6](https://doi.org/10.1016/S0924-7963(02)00072-6), 2002.
- 1028 Álvarez, E., Morán, X. A. G., López-Urrutia, Á., and Nogueira, E.: Size-dependent
1029 photoacclimation of the phytoplankton community in temperate shelf waters (southern
1030 Bay of Biscay), *Mar. Ecol. Prog. Ser.*, 543, 73–87, <https://doi.org/10.3354/meps11580>,
1031 2016.
- 1032 Antoine, D., Morel, A., and André, J.-M.: Algal pigment distribution and primary production
1033 in the eastern Mediterranean as derived from coastal zone color scanner observations, *J.*
1034 *Geophys. Res.*, 100, 16193–16209, <https://doi.org/10.1029/95JC00466>, 1995.
- 1035 Antoine, D., André, J.-M., and Morel, A.: Oceanic primary production: 2. Estimation at global
1036 scale from satellite (Coastal Zone Color Scanner) chlorophyll, *Global Biogeochem. Cy.*,
1037 10, 57–69, <https://doi.org/10.1029/95GB02832>, 1996.
- 1038 Antoine, D., D’Ortenzio, F., Hooker, S. B., Bécu, G., Gentili, B., Tailliez, D., and Scott, A. J.:
1039 Assessment of uncertainty in the ocean reflectance determined by three satellite ocean
1040 color sensors (MERIS, SeaWiFS and MODIS-A) at an offshore site in the Mediterranean
1041 Sea (BOUSSOLE project), *J. Geophys. Res.*, 113, 1–22,
1042 <https://doi.org/10.1029/2007JC004472>, 2008.
- 1043 Barber, R. T., and Hitling, A. K.: History of the study of plankton productivity, in:
1044 *Phytoplankton Productivity: Carbon assimilation in marine and freshwater ecosystems*,

1045 edited by Williams, P. J. le B., Thomas, D. N., and Reynolds, C. S., Blackwell Science,
1046 Oxford, 16–43, <https://doi.org/10.1002/9780470995204>, 2002.

1047 Barbieux, M., Uitz, J., Bricaud, A., Organelli, E., Poteau, A., Schmechtig, C., Gentili, B.,
1048 Penker'h, C., Leymarie, E., D'Ortenzio, F., and Claustre, H.: Assessing the variability
1049 in the relationship between the particulate backscattering coefficient and the chlorophyll
1050 a concentration from a global Biogeochemical-Argo database, *J. Geophys. Res.*, 123,
1051 1229–1250, <https://doi.org/10.1002/2017JC013030>, 2017.

1052 Barbieux, M., Uitz, J., Gentili, B., Pasqueron de Fommervault, O., Mignot, A., Poteau, A.,
1053 Schmechtig, C., Taillandier, V., Leymarie, E., Penker'h, C., D'Ortenzio, F., Claustre,
1054 H., and Bricaud, A.: Bio-optical characterization of subsurface chlorophyll maxima in the
1055 Mediterranean Sea from a Biogeochemical-Argo float database, *Biogeosciences*, 16,
1056 1321–1342, <https://doi.org/10.5194/bg-16-1321-2019>, 2019.

1057 Barnes, M., and Antoine, D.: Proxies of community production derived from the diel variability
1058 of particulate attenuation and backscattering coefficients in the northwest mediterranean
1059 sea, *Limnol. Oceanogr.*, 59, 2133–2149, <https://doi.org/10.4319/lo.2014.59.6.2133>,
1060 2014.

1061 Beckmann, A. and Hense, I.: Beneath the surface: Characteristics of oceanic ecosystems under
1062 weak mixing conditions – A theoretical investigation, *Prog. Oceanogr.*, 75, 771–796,
1063 <https://doi.org/10.1016/j.pocean.2007.09.002>, 2007.

1064 Behrenfeld, M. J., and Boss, E.: The beam attenuation to chlorophyll ratio: an optical index of
1065 phytoplankton physiology in the surface ocean?, *Deep-Sea Res. Pt. I*, 50, 1537–1549,
1066 <https://doi.org/10.1016/j.dsr.2003.09.002>, 2003.

1067 Behrenfeld, M. J., and Boss, E.: Beam attenuation and chlorophyll concentration as alternative
1068 optical indices of phytoplankton biomass, *J. Mar. Res.*, 64, 431–451,
1069 <https://doi.org/10.1357/002224006778189563>, 2006.

1070 Behrenfeld, M. J., Marañón, E., Siegel, D. A., and Hooker, S. B.: Photoacclimation and
1071 nutrient-based model of light-saturated photosynthesis for quantifying oceanic primary
1072 production, *Mar. Ecol. Prog. Ser.*, 228, 103–117, <https://doi.org/10.3354/meps228103>,
1073 2002.

1074 Bernard, S., Probyn, T. A., and Quirantes, A.: Simulating the optical properties of
1075 phytoplankton cells using a two-layered spherical geometry, *Biogeosciences Discuss.*, 6,
1076 1497–1563, <https://doi.org/10.5194/bgd-6-1497-2009>, 2009.

1077 Bethoux, J. P., Morin, P., Madec, C., and Gentili, B.: Phosphorus and nitrogen behaviour in the
1078 Mediterranean Sea, *Deep-Sea Res.*, 39, 1641–1654, [https://doi.org/10.1016/0198-](https://doi.org/10.1016/0198-0149(92)90053-V)
1079 [0149\(92\)90053-V](https://doi.org/10.1016/0198-0149(92)90053-V), 1992.

1080 Bosc, E., Bricaud, A., and Antoine, D.: Seasonal and interannual variability in algal biomass
1081 and primary production in the Mediterranean Sea, as derived from 4 years of SeaWiFS
1082 observations, *Global Biogeochem. Cy.* 18, GB1005,
1083 <https://doi.org/10.1029/2003GB002034>, 2004.

1084 Boss, E., Pegau, W. S., Lee, M., Twardowski, M., Shybanov, E., Korotaev, G., and Baratange,
1085 F.: Particulate backscattering ratio at LEO 15 and its use to study particle composition
1086 and distribution, *J. Geophys. Res.*, 109, C01014, <https://doi.org/10.1029/2002JC001514>,
1087 2004.

1088 Boss., E., and Zaneveld, J. R. V.: The effect of bottom substrate on inherent optical properties:
1089 Evidence of biogeochemical processes. *Limnol. Oceanogr.*, 48, 346–354.
1090 https://doi.org/10.4319/lo.2003.48.1_part_2.0346, 2003.

1091 Bricaud, A., Morel, A., and Prieur, L.: Absorption by dissolved organic matter of the sea
1092 (yellow substance) in the UV and visible domains, *Limnol. Oceanogr.*, 26,
1093 <https://doi.org/10.4319/lo.1981.26.1.0043>, 1981.

1094 Briggs, N., Perry, M. J., Cetinić, I., Lee, C., D'Asaro, E., Gray, A. M., Rehm, E.: High-
1095 resolution observations of aggregate flux during a sub-polar North Atlantic spring bloom,
1096 *Deep-Sea Res. Pt. I*, 58, 1031–1039, <https://doi.org/10.1016/j.dsr.2011.07.007>, 2011.

1097 Briggs, N., Guðmundsson, K., Cetinić, I., D'Asaro, E., Rehm, E., Lee, C., and Perry, M. J.: A
1098 multi-method autonomous assessment of primary productivity and export efficiency in
1099 the springtime North Atlantic, *Biogeosciences*, 15, 4515–4532,
1100 <https://doi.org/10.5194/bg-15-4515-2018>, 2018.

1101 Brunet C., Casotti R., Vantrepotte V., and Conversano F.: Vertical variability and diel dynamics
1102 of picophytoplankton in the Strait of Sicily, Mediterranean Sea, in summer, *Mar. Ecol.*
1103 *Prog. Ser.*, 346, 15–26, <https://doi.org/10.3354/meps07017>, 2007.

1104 [Brunet, C., Casotti, R., and Vantrepotte, V.: Phytoplankton diel and vertical variability in](#)
1105 [photobiological responses at a coastal station in the Mediterranean Sea, *J Plank Res.* 30,](#)
1106 [645–654, <https://doi.org/10.1093/plankt/fbn028>, 2008.](#)

1107 Casotti, R., Landolfi, A., Brunet, C., D'Ortenzio, F., Mangoni, O., and Ribera d'Alcalá, M.:
1108 Composition and dynamics of the phytoplankton of the Ionian Sea (eastern
1109 Mediterranean), *J. Geophys. Res.*, 108, 1–19, <https://doi.org/10.1029/2002JC001541>,
1110 2003.

1111 Cetinić, I., Perry, M. J., Briggs, N. T., Kallin, E., D'Asaro, E. A., and Lee, C. M.: Particulate
1112 organic carbon and inherent optical properties during 2008 North Atlantic Bloom
1113 Experiment, *J. Geophys. Res.*, 117, 1–18, <https://doi.org/10.1029/2011JC007771>, 2012.

1114 Cetinić, I., Perry, M. J., D'Asaro, E., Briggs, N., Poulton, N., Sieracki, M. E., and Lee, C. M.:
1115 A simple optical index shows spatial and temporal heterogeneity in phytoplankton
1116 community composition during the 2008 North Atlantic Bloom Experiment,
1117 *Biogeosciences*, 12, 2179–2194, <https://doi.org/10.5194/bg-12-2179-2015>, 2015.

1118 Chavez F. P., Messié, M., and Pennington, J. T.: Marine Primary Production in Relation to
1119 Climate Variability and Change, *Annual Rev. Mar. Sci.*, 3, 227–260,
1120 <https://doi.org/10.1146/annurev.marine.010908.163917>, 2013.

1121 Claustre, H.: The trophic status of various oceanic provinces as revealed by phytoplankton
1122 pigment signatures, *Limnol. Oceanogr.*, 39, 1206–1210, 39,
1123 <https://doi.org/10.4319/lo.1994.39.5.1206>, 2014.

1124 Claustre, H., Bricaud, A., Babin, M., Bruyant, F., Guillou, L., Le Gall, F., Marie, D., Partensky,
1125 F.: Diel variations in Prochlorococcus optical properties, *Limnol. Oceanogr.*, 47, 1637–
1126 1647, <https://doi.org/10.4319/lo.2002.47.6.1637>, 2002.

1127 Claustre, H., Huot, Y., Obernosterer, I., Gentili, B., Tailliez, D., and Lewis, M.: Gross
1128 community production and metabolic balance in the South Pacific Gyre, using a non
1129 intrusive bio-optical method, *Biogeosciences*, 5, 463–474, [https://doi.org/10.5194/bg-5-](https://doi.org/10.5194/bg-5-463-2008)
1130 463-2008, 2008.

1131 Cloern, J. E.: The relative importance of light and nutrient limitation of phytoplankton growth:
1132 A simple index of coastal ecosystem sensitivity to nutrient enrichment, *Aquat. Ecol.*, 33,
1133 3–16, <https://doi.org/10.1023/A:1009952125558>, 1999.

1134 Cornec, M., Claustre, H., Mignot, A., Guidi, L., Lacour, L., Poteau, A., D'Ortenzio, F., Gentili,
1135 B., and Schmechtig, C.: Deep chlorophyll maxima in the global ocean: occurrences,
1136 drivers and characteristics, *Global Biogeochem. Cy.*, 35, e2020GB006759,
1137 <https://doi.org/10.1029/2020GB006759>, 2021.

1138 [Corno, G., Letelier, R.M., Abbott, M. R., and Karl, D.M.: Assessing primary production](#)
1139 [variability in the North Pacific Subtropical Gyre: A comparison of Fast Repetition Rate](#)
1140 [Fluorometry and ¹⁴C measurements, J. Phycol., 42, \[https://doi.org/10.1111/j.1529-\]\(https://doi.org/10.1111/j.1529-8817.2006.00163.x\)](#)
1141 [8817.2006.00163.x, 2005.](#)

1142 Crombet, Y., Leblanc, K., Quéguiner, B., Moutin, T., Rimmelin, P., Ras, J., Claustre, H.,
1143 Leblond, N., Oriol, L., and Pujol-Pay, M.: Deep silicon maxima in the stratified
1144 oligotrophic Mediterranean Sea, *Biogeosciences*, 8, 459–475, [https://doi.org/10.5194/bg-](https://doi.org/10.5194/bg-8-459-2011)
1145 8-459-2011, 2011.

1146 Cullen, J. J.: The deep chlorophyll maximum: comparing vertical profiles of chlorophyll a, *Can.*
1147 *J. Fish. Aquat. Sci.*, 39, 791–803, <https://doi.org/10.1139/f82-108>, 1982.

1148 Cullen, J. J., Lewis, M. R., Davis, C. O., and Barber, R. T.: Photosynthetic characteristics and
1149 estimated growth rates indicate grazing is the proximate control of primary production in
1150 the equatorial Pacific, *J. Geophys. Res.*, 97, 639–654,
1151 <https://doi.org/10.1029/91JC01320>, 1992.

1152 Cullen, J. J., and Lewis, M. R.: Biological processes and optical measurements near the sea
1153 surface: Some issues relevant to remote sensing, *J. Geophys. Res.*, 100(C7), 13255–
1154 13266, <https://doi.org/10.1029/95JC00454>, 1995.

1155 Cullen, J. J.: Subsurface chlorophyll maximum layers: enduring enigma or mystery solved?,
1156 *Ann Rev Mar Sci.*, 7, 207-39, <https://doi.org/10.1146/annurev-marine-010213-135111>,
1157 2015.

1158 Dandonneau, Y.: Measurement of in situ profiles of primary production using an automated
1159 sampling and incubation device, *ICES Mar. Sci. Sym.*, 197, 172–180, 1993.

1160 de Boyer Montégut, C., Madec, G., Fischer, A. S., Lazar, A., and Iudicone, D.: Mixed layer
1161 depth over the global ocean: An examination of profile data and a profile-based
1162 climatology, *J. Geophys. Res.*, 109, 1–20, <https://doi.org/10.1029/2004JC002378>, 2004.

1163 del Giorgio P. A., and Duarte C. M.: Respiration in the open ocean, *Nature*, 420, 37984.
1164 <https://doi.org/10.1038/nature01165>, 2002.

1165 Di Cicco, A., Sammartino, M., Marullo, S., and Santoleri, R.: Regional empirical algorithms for
1166 an improved identification of phytoplankton functional types and size classes in the
1167 Mediterranean Sea using satellite data, *Frontiers Mar. Sci.*, 4126, 1–18, [https://doi.org/](https://doi.org/10.3389/fmars.2017.00126)
1168 [10.3389/fmars.2017.00126](https://doi.org/10.3389/fmars.2017.00126), 2017.

1169 D'Ortenzio, F. and Ribera d'Alcalà, M.: On the trophic regimes of the Mediterranean Sea: a
1170 satellite analysis, *Biogeosciences*, 6, 139–148, <https://doi.org/10.5194/bg-6-139-2009>,
1171 2009.

1172 Duarte, C. M., and Agusti S.: The CO₂ balance of unproductive aquatic ecosystems, *Science*,
1173 281, 234–6, <https://doi.org/10.1126/science.281.5374.234>, 1998.

1174 Dubinsky, Z., and Stambler, N.: Photoacclimation processes in phytoplankton: mechanisms,
1175 consequences, and applications, *Aquat. Microb. Ecol.*, 56,163–176,
1176 <https://doi.org/10.3354/ame01345>, 2009.

1177 Dugdale, R. C., and Wilkerson, F. P.: Nutrient sources and primary production in the Eastern
1178 Mediterranean, *Oceanologica Acta*, 1988.

1179 Durand, M. D., and Olson, R. J.: Contributions of phytoplankton light scattering and cell
1180 concentration changes to diel variations in beam attenuation in the equatorial pacific from
1181 flow cytometric measurements of pico-, ultra and nanoplankton, *Deep-Sea Res. Pt. II*, 43,
1182 891–906, [https://doi.org/10.1016/0967-0645\(96\)00020-3](https://doi.org/10.1016/0967-0645(96)00020-3), 1996.

1183 Durand, M. D., and Olson, R.J.: Diel patterns in optical properties of the chlorophyte
1184 *Nannochloris* sp.: Relating individual-cell to bulk measurements, *Limnol. Oceanogr.*, 43,
1185 1107–1118, <https://doi.org/10.4319/lo.1998.43.6.1107>, 1998.

1186 Durand, M. D. Green, R. E., Sosik, H. M. and Olson, R. J.: Diel Variations in Optical Properties
1187 of *Micromonas Pusilla* (Prasinophyceae), *J. Phycol.*, 38, 1132–1142,
1188 <https://doi.org/10.1046/j.1529-8817.2002.02008.x>, 2002.

1189 Estapa, M. L., Buessler, K., Boss, E., and Gerbi, G.: Autonomous, high-resolution
1190 observations of particle flux in the oligotrophic ocean, *Biogeosciences*, 10, 5517–5531,
1191 <https://doi.org/10.5194/bg-10-5517-2013>, 2013.

1192 Falkowski, P. G.: Ocean Science: The power of plankton, *Nature*, 483, S17–S20,
1193 <https://doi.org/10.1038/483S17a>, 2012.

1194 Fennel, K., and Boss, E.: Subsurface maxima of phytoplankton and chlorophyll: Steady-state
1195 solutions from a simple model, *Limnol. Oceanogr.*, 48, 1521–1534,
1196 <https://doi.org/10.4319/lo.2003.48.4.1521>, 2003.

1197 Field, C. B., Behrenfeld, M. J., Randerson, J. T., and Falkowski, P.: Primary production of the
1198 biosphere: integrating terrestrial and oceanic components, *Science* 281, 237–240,
1199 <https://doi.org/10.1126/science.281.5374.237>, 1998.

1200 Fitzwater, S.E., Knauer, G.A., and Martin, J.H.: Metal contamination and its effect on primary
1201 production measurements, *Limnol. Oceanogr.*, 27, 44–551,
1202 <https://doi.org/10.4319/lo.1982.27.3.0544>, 1982.

1203 Gardner, W. D., Mishonov, A. V., and Richardson, M. J.: Global POC concentrations from in-
1204 situ and satellite data, *Deep-Sea Res. Pt. II*, 53, 718–740,
1205 <https://doi.org/10.1016/j.dsr2.2006.01.029>, 2006.

1206 Geider, R. J.: Light and temperature dependence of the carbon to chlorophyll a ratio in
1207 microalgae and cyanobacteria: Implications for physiology and growth of phytoplankton,
1208 *New Phytol.*, 106, 1–34, <https://doi.org/10.1111/j.1469-8137.1987.tb04788.x>, 1987.

1209 Geider, R. J., MacIntyre, H. L., and Kana T. M.: Dynamic model of phytoplankton growth and
1210 acclimation: Responses of the balanced growth rate and the chlorophyll a:carbon ratio to
1211 light, nutrient-limitation and temperature, *Mar. Ecol. Prog. Ser.*, 148, 187–200,
1212 <https://doi.org/10.3354/meps148187>, 1997.

1213 Gernez, P., Antoine, D., and Huot, Y.: Diel cycles of the particulate beam attenuation
1214 coefficient under varying trophic conditions in the northwestern Mediterranean Sea:
1215 Observations and modeling, *Limnol. Oceanogr.*, 56, 17–36,
1216 <https://doi.org/10.4319/lo.2011.56.1.0017>, 2011.

1217 Gitelson, A., Karnieli, A., Goldman, N., Yacobi, Y.Z., and Mayo, M.: Chlorophyll estimation
1218 in the Southeastern Mediterranean using CZCS images: adaptation of an algorithm and
1219 its validation, *J. Mar. Syst.*, 9, 283–290, [https://doi.org/10.1016/S0924-7963\(95\)00047-](https://doi.org/10.1016/S0924-7963(95)00047-X)
1220 [X](https://doi.org/10.1016/S0924-7963(95)00047-X), 1996.

1221 Guieu, C., D'Ortenzio, F., Dulac, F., Taillandier, V., Doglioli, A., Petrenko, A., Barrillon, S.,
1222 Mallet, M., Nabat, P., and Desboeufs, K.: Introduction: Process studies at the air–sea
1223 interface after atmospheric deposition in the Mediterranean Sea – objectives and strategy
1224 of the PEACETIME oceanographic campaign (May–June 2017), *Biogeosciences*, 17,
1225 5563–5585, <https://doi.org/10.5194/bg-17-5563-2020>, 2020.

1226 González, N., Anadón, R., Mouriño, B., Fernández, E., Sinha, B., Escánez, J., and de Armas,
1227 D.: The metabolic balance of the planktonic community in the North Atlantic Subtropical
1228 Gyre: The role of mesoscale instabilities, *Limnol. Oceanogr.*, 4,
1229 <https://doi.org/10.4319/lo.2001.46.4.0946>, 2001.

- 1230 González, N., Anadón, R., and Marañón, E.: Large-scale variability of planktonic net
1231 community metabolism in the Atlantic Ocean: Importance of temporal changes in
1232 oligotrophic subtropical waters, *Mar. Ecol. Progr. Ser.*, 233, 21–30,
1233 <https://doi.org/10.3354/meps233021>, 2002.
- 1234 Gordon, H. R., and McCluney, W. R.: Estimation of the Depth of Sunlight Penetration in the
1235 Sea for Remote Sensing, *Appl. Opt.*, 14, 413–416,
1236 <https://doi.org/10.1364/AO.14.000413>, 1975.
- 1237 Hense, I., and Beckmann, A.: Revisiting subsurface chlorophyll and phytoplankton
1238 distributions, *Deep-Sea Res. Pt. I*, 55, 1193–1199,
1239 <https://doi.org/10.1016/j.dsr.2008.04.009>, 2008.
- 1240 Jacquet, S., Lennon, J.-F., Marie, D., and Vaultot, D.: Picoplankton population dynamics in
1241 coastal waters of the northwestern Mediterranean Sea, *Limnol. Oceanogr.*, 43, 1916–
1242 1931, <https://doi.org/10.4319/lo.1998.43.8.1916>, 1998.
- 1243 Juranek, L. W., and Quay, P. D.: In vitro and in situ gross primary and net community
1244 production in the North Pacific Subtropical Gyre using labeled and natural abundance
1245 isotopes of dissolved O₂, *Glob. Biogeochem. Cy.*, 19,
1246 <https://doi.org/10.1029/2004GB002384>, 2005.
- 1247 Karl, D. M., Laws, E. A., Morris, P., Williams, P. J. le B., and Emerson, S.: Metabolic balance
1248 of the open sea, *Nature*, 426, 32–32, <https://doi.org/10.1038/426032a>, 2003.
- 1249 Kemp, A. E. S., and Villareal, T. A.: High diatom production and export in stratified waters -
1250 A potential negative feedback to global warming, *Prog. Oceanogr.*, 119, 4–23,
1251 <https://doi.org/10.1016/j.pocean.2013.06.004>, 2013.

1252 Kemp, A. E. S., and Villareal, T. A.: The case of the diatoms and the muddled mandalas: Time
1253 to recognize diatom adaptations to stratified waters, *Prog. Oceanogr.*, 167, 138-149,
1254 <https://doi.org/10.1016/j.pocean.2018.08.002>, 2018.

1255 Kheireddine, M., and Antoine, D.: Diel variability of the beam attenuation and backscattering
1256 coefficients in the northwestern Mediterranean Sea (BOUSSOLE site), *J. Geophys. Res.*,
1257 119, 5465– 5482, <https://doi.org/10.1002/2014JC010007>, 2014.

1258 Kiefer, D. A., Olson, R. J., and Holm-Hansen, O.: Another look at the nitrite and chlorophyll
1259 maxima in the central North Pacific, *Deep-Sea Res.*, 23, 1199–1208,
1260 [https://doi.org/10.1016/0011-7471\(76\)90895-0](https://doi.org/10.1016/0011-7471(76)90895-0), 1976.

1261 [Kolber, Z. S., and Falkowski, P. G.: Use of active fluorescence to estimate phytoplankton](#)
1262 [photosynthesis in-situ, *Limnol. Oceanogr.*, 38, 1646–1665, 1993.](#)

1263 Lacroix, G., and Nival, P.: Influence of meteorological variability on primary production
1264 dynamics in the Ligurian Sea (NW Mediterranean Sea) with a 1D
1265 hydrodynamic/biological model, *J. Mar. Syst.*, 16, 23–50, [https://doi.org/10.1016/S0924-](https://doi.org/10.1016/S0924-7963(97)00098-5)
1266 [7963\(97\)00098-5](https://doi.org/10.1016/S0924-7963(97)00098-5), 1998.

1267 Lavigne, H., D'Ortenzio, F., Migon, C., Claustre, H., Testor, P., Ribera d'Alcalà, M., Lavezza,
1268 R., Houpert, L., and Prieur, L.: Enhancing the comprehension of mixed layer depth
1269 control on the Mediterranean phytoplankton phenology, *J. Geophys. Res. Oceans*, 118,
1270 3416–3430, <https://doi.org/10.1002/jgrc.2025>, 2013.

1271 Lavigne, H., D'Ortenzio, F., Ribera D'Alcalà, M., Claustre, H., Sauzède, R., and Gacic, M.: On
1272 the vertical distribution of the chlorophyll a concentration in the Mediterranean Sea: a
1273 basin-scale and seasonal approach, *Biogeosciences*, 12, 5021–5039,
1274 <https://doi.org/10.5194/bg-12-5021-2015>, 2015.

- 1275 Letelier, R. M., Karl, D. M., Abbott, M. R., Bidigare, R. R.: Light driven seasonal patterns of
1276 chlorophyll and nitrate in the lower euphotic zone of the North Pacific Subtropical Gyre,
1277 *Limnol. Oceanogr.*, 2, 508–519, <https://doi.org/10.4319/lo.2004.49.2.0508>, 2004.
- 1278 [Litaker, R.W., Warner, V., Rhyne, C.F., Duke, C.S., Kenney, B.E., Ramus, J., and Tester, P.A.:](#)
1279 [Effect of diel and interday variations in light on the cell division pattern and in situ growth](#)
1280 [rates of the bloom-forming dinoflagellate *Heterocapsa triquetra*. *Mar Ecol Prog Ser*, 232,](#)
1281 [63–74, <https://doi.org/10.3354/MEPS232063>, 2002.](#)
- 1282 Loisel, H., Mériaux, X., Berthon, J.-F., Poteau, A.: Investigation of the optical backscattering
1283 to scattering ratio of marine particles in relation to their biogeochemical composition in
1284 the eastern English Channel and southern North Sea, *Limnol. Oceanogr.*, 52, 739–752,
1285 <https://doi.org/10.4319/lo.2007.52.2.0739>, 2007.
- 1286 Loisel, H., Vantrepotte, V., Norkvist, K., Mériaux, X., Kheireddine, M., Ras, J., Pujo-Pay, M.,
1287 Combet, Y., Leblanc, K., Dall'Olmo, G., Mauriac, R., Dessailly, D., and Moutin, T.:
1288 Characterization of the bio-optical anomaly and diurnal variability of particulate matter,
1289 as seen from scattering and backscattering coefficients, in ultra-oligotrophic eddies of the
1290 Mediterranean Sea, *Biogeosciences*, 8, 3295–3317, [https://doi.org/10.5194/bg-8-3295-](https://doi.org/10.5194/bg-8-3295-2011)
1291 2011, 2011.
- 1292 Longhurst, A., Sathyendranath, S., Platt, T., and Caverhill, C.: An estimate of global primary
1293 production in the ocean from satellite radiometer data, *J. Plank. Res.*, 17, 1245–1271,
1294 <https://doi.org/10.1093/plankt/17.6.1245>, 1995.
- 1295 Magazzu, G., and Decembrini, F.: Primary production, biomass and abundance of phototrophic
1296 picoplankton in the Mediterranean Sea: A review, *Aquat. Microb. Ecol.*, 9, 97– 104,
1297 <https://doi.org/10.3354/ame009097>, 1995.

1298 Marañón, E., Van Wambeke, F., Uitz, J., Boss, E. S., Dimier, C., Dinasquet, J., Engel, A.,
1299 Haëntjens, N., Pérez-Lorenzo, M., Taillandier, V., and Zäncker, B.: Deep maxima of
1300 phytoplankton biomass, primary production and bacterial production in the
1301 Mediterranean Sea, *Biogeosciences*, 18, 1749–1767, [https://doi.org/10.5194/bg-18-1749-](https://doi.org/10.5194/bg-18-1749-2021)
1302 2021, 2021.

1303 Marra, J., Langdon, C., and Knudson, C. A.: Primary production, water column changes, and
1304 the demise of a *Phaeocystis* bloom at the Marine Light-Mixed Layers site (59°N, 21°W)
1305 in the northeast Atlantic Ocean, *J. Geophys. Res.*, 100, 6633–6643,
1306 <https://doi.org/10.1029/94JC01127>, 1995.

1307 Marty, J. C., Chiavérini, J., Pizay, M. D., and Avril, B.: Seasonal and interannual dynamics of
1308 nutrients and phytoplankton pigments in the western Mediterranean Sea at the
1309 DYFAMED time-series station (1991–1999), *Deep-Sea Res. Pt. II*, 49, 1965–1985,
1310 [https://doi.org/10.1016/S0967-0645\(02\)00022-X](https://doi.org/10.1016/S0967-0645(02)00022-X), 2002.

1311 Marty, J. C. and Chiavérini, J.: Hydrological changes in the Ligurian Sea (NW Mediterranean,
1312 DYFAMED site) during 1995–2007 and biogeochemical consequences, *Biogeosciences*,
1313 7, 2117–2128, <https://doi.org/10.5194/bg-7-2117-2010>, 2010.

1314 Mayot, N., D'Ortenzio, F., Ribera d'Alcalà, M., Lavigne, H., and Claustre, H.: Interannual
1315 variability of the Mediterranean trophic regimes from ocean color satellites,
1316 *Biogeosciences*, 13, 1901–1917, <https://doi.org/10.5194/bg-13-1901-2016>, 2016.

1317 McClain, C. R., Signorini, S. R., and Christian, J. R.: Subtropical gyre variability observed by
1318 ocean-color satellites, *Deep-Sea Res. Pt. II*, 51, 281–301,
1319 <https://doi.org/10.1016/j.dsr2.2003.08.002>, 2004.

1320 McGillicuddy Jr., D. J.: Mechanisms of Physical-Biological-Biogeochemical Interaction at the
1321 Oceanic Mesoscale, *Annu. Rev. Mar. Sci.*, 8–1, 125–159, 2016.

1322 Mignot, A., Claustre, H., Uitz, J., Poteau, A., D'Ortenzio, F., and Xing, X.: Understanding the
1323 seasonal dynamics of phytoplankton biomass and the deep chlorophyll maximum in
1324 oligotrophic environments: A Bio-Argo float investigation, *Global Biogeochem. Cy.*, 28,
1325 856– 876, <https://doi.org/10.1002/2013GB004781>, 2014.

1326 Minas, H. J.: La distribution de l'oxygène en relation avec la production primaire en
1327 Méditerranée Nord-Occidentale, *Mar. Biol.*, 7, 181–204,
1328 <https://doi.org/10.1007/BF00367489>, 1970.

1329 Morel, A.: Light and marine photosynthesis: a spectral model with geochemical and
1330 climatological implications, *Prog. Oceanogr.*, 26, 263–306, [https://doi.org/10.1016/0079-](https://doi.org/10.1016/0079-6611(91)90004-6)
1331 [6611\(91\)90004-6](https://doi.org/10.1016/0079-6611(91)90004-6), 1991.

1332 Morel, A., and André, J.-M.: Pigment distribution and primary production in the western
1333 Mediterranean as derived and modeled from coastal zone color scanner observations, *J.*
1334 *Geophys. Res.*, 96, 12685– 12698, <https://doi.org/10.1029/91JC00788>, 1991.

1335 Morel, A., Antoine, D., Babin, M., and Dandonneau, Y.: Measured and modeled primary
1336 production in the northeast Atlantic (EUMELI JGOFS program): the impact of natural
1337 variations in photosynthetic parameters on model predictive skill, *Deep-Sea Res. Pt. I*,
1338 43, 1273–1304, [https://doi.org/10.1016/0079-6611\(91\)90004-6](https://doi.org/10.1016/0079-6611(91)90004-6), 1996.

1339 Moutier, W., Duforêt-Gaurier, L., Thyssen, M., Loisel, H., Mériaux, X., Courcot, L., Dessailly,
1340 D., Réve, M.-H., Grégori, G., Alvain, S., Barani, A., Brutier, L., and Dugrune, M.:
1341 Evolution of the scattering properties of phytoplankton cells from flow cytometry
1342 measurements, *PLOS ONE*, 12, e0181180,
1343 <https://doi.org/10.1371/journal.pone.0181180>, 2017.

1344 Neukermans, G., Loisel, H., Mériaux, X., Astoreca, R., and McKee, D.: In situ variability of
1345 mass-specific beam attenuation and backscattering of marine particles with respect to

1346 particle size, density, and composition, *Limnol. Oceanogr.*, 57, 124–144,
1347 <https://doi.org/10.4319/lo.2012.57.1.0124>, 2012.

1348 Nielsen, E. S.: The Use of radio-active carbon (C^{14}) for measuring organic production in the
1349 sea, *ICES J. Mar. Sci.*, 18, 117–140, <https://doi.org/10.1093/icesjms/18.2.117>, 1952.

1350 Organelli, E., Barbicux, M., Claustre, H., Schmechtig, C., Poteau, A., Bricaud, A., Boss, E.,
1351 Briggs, N., Dall'Olmo, G., D'Ortenzio, F., Leymarie, E., Mangin, A., Obolensky, G.,
1352 Penkerch, C., Prieur, L., Roesler, C., Serra, R., Uitz, J., and Xing, X.: Two databases
1353 derived from BGC-Argo float measurements for marine biogeochemical and bio-optical
1354 applications, *Earth Syst. Sci. Data*, 9, 861–880, <https://doi.org/10.5194/essd-9-861-2017>,
1355 2017.

1356 Organelli, E., Dall'Olmo, G., Brewin, R. J. W., Taran, G., Boss, E., and Bricaud, A.: The open-
1357 ocean missing backscattering is in the structural complexity of particles, *Nat. Commun.*,
1358 9, 5439, <https://doi.org/10.1038/s41467-018-07814-6>, 2018.

1359 Oubelkheir, K., Claustre, H., Sciandra, A., and Babin, M.: Bio-optical and biogeochemical
1360 properties of different trophic regimes in oceanic waters, *Limnol. Oceanogr.*, 50, 1795–
1361 1809, <https://doi.org/10.4319/lo.2005.50.6.1795>, 2015.

1362 [Oubelkheir, K. and Sciandra, A.: Diel variations in particle stocks in the oligotrophic waters](#)
1363 [of the Ionian Sea \(Mediterranean\), *J. Mar. Syst.*, 74, 1–2,](#)
1364 <https://doi.org/10.1016/j.jmarsys.2008.02.008>, 2008.

1365 Pasqueron de Fommervault, O., Migon, C., D'Ortenzio, F., Ribera d'Alcalà, M, and Coppola,
1366 L.: Temporal variability of nutrient concentrations in the northwestern Mediterranean Sea
1367 (DYFAMED time-series station), *Deep-Sea Res. Pt. I*, 100, 1–12,
1368 <https://doi.org/10.1016/j.dsr.2015.02.006>, 2015.

1369 Polovina, J. J., Howell, E. A., and Abecassis, M.: Ocean's least productive waters are
1370 expanding, *Geophys. Res. Lett.*, 35, L03618, <https://doi.org/10.1029/2007GL031745>,
1371 2008.

1372 Quay, P. D., Peacock, C., Björkman, K., and Karl, D. M.: Measuring primary production rates
1373 in the ocean: Enigmatic results between incubation and non-incubation methods at Station
1374 ALOHA, *Glob. Biogeochem. Cy.*, 24, <https://doi.org/10.1029/2009GB003665>, 2010.

1375 Ras, J., Claustre, H., and Uitz, J.: Spatial variability of phytoplankton pigment distributions in
1376 the Subtropical South Pacific Ocean: comparison between in situ and predicted data,
1377 *Biogeosciences*, 5, 353–369, <https://doi.org/10.5194/bg-5-353-2008>, 2008.

1378 [Regaudie-de-Gioux, A., Lasternas, S., Agustí, S., and Duarte, C. M.: Comparing marine](#)
1379 [primary production estimates through different methods and development of conversion](#)
1380 [equations, *Frontiers*, 1, <https://doi.org/10.3389/fmars.2014.00019>, 2014.](#)

1381 Roesler, C. S. and Boss, E.: In Situ Measurement of the Inherent Optical Properties (IOPs) and
1382 Potential for Harmful Algal Bloom Detection and Coastal Ecosystem Observations. *In*
1383 Babin, M., Roesler, C. S. and Cullen, J. J., Real-time coastal observing systems for marine
1384 ecosystem dynamics and harmful algal blooms: Theory, instrumentation and modelling.
1385 UNESCO, 2008.

1386 Roesler, C., Uitz, J., Claustre, H., Boss, E., Xing, X., Organelli, E., Briggs, N., Bricaud, A.,
1387 Schmechtig, C., Poteau, A., D'Ortenzio, F., Ras, J., Drapeau, S., Haëntjens, N. and
1388 Barbieux, M.: Recommendations for obtaining unbiased chlorophyll estimates from in
1389 situ chlorophyll fluorometers: A global analysis of WET Labs ECO sensors, *Limnol.*
1390 *Oceanogr.-Meth.*, 15, 572–585, <https://doi.org/10.1002/lom3.10185>, 2017.

1391 Saba, V.S., Friedrichs, M. A. M., Carr, M.-E., et al.: Challenges of modeling depth-integrated
1392 marine primary productivity over multiple decades: A case study at BATS and HOT,
1393 *Glob. Biogeochem. Cy.*, 24, doi: 10.1029/2009GB003655, 2010.

1394 Saba, V. S., Friedrichs, M. A. M., Antoine, D., Armstrong, R. A., Asanuma, I., Behrenfeld, M.
1395 J., Ciotti, A. M., Dowell, M., Hoepffner, N., Hyde, K. J. W., Ishizaka, J., Kameda, T.,
1396 Marra, J., Mélin, F., Morel, A., O'Reilly, J., Scardi, M., Smith Jr., W. O., Smyth, T. J.,
1397 Tang, S., Uitz, J., Waters, K., and Westberry, T. K.: An evaluation of ocean color model
1398 estimates of marine primary productivity in coastal and pelagic regions across the globe,
1399 *Biogeosciences*, 8, 489–503, <https://doi.org/10.5194/bg-8-489-2011>, 2011.

1400 Sarmiento, J. L., and Siegenthaler, U.: New production and the global carbon cycle, in: Primary
1401 productivity and biogeochemical cycles in the sea, *Environmental Science Research*, vol.
1402 43, edited by Falkowski, P. G., Woodhead A. D., and Vivirito K., Springer, Boston, MA,
1403 https://doi.org/10.1007/978-1-4899-0762-2_18, 1992.

1404 Sarmiento, J. L., Slater, R., Barber, R., Bopp, L., Doney, S. C., Hirst, A. C., Kleypas, J., Matear,
1405 R., Mikolajewicz, U., Monfray, P., Soldatov, V., Spall, S. A., and Stouffer, R.: Response
1406 of ocean ecosystems to climate warming, *Global Biogeochem. Cy.*, 18, 1–23,
1407 <https://doi.org/10.1029/2003GB002134>, 2014.

1408 Sathyendranath, S., Longhurst, A., Caverhill, C. M., and Platt, T.: Regionally and Seasonally
1409 Differentiated Primary Production in the North Atlantic, *Deep-Sea Res. Pt. I*, 42, 1773–
1410 1802, [https://doi.org/10.1016/0967-0637\(95\)00059-F](https://doi.org/10.1016/0967-0637(95)00059-F), 1995.

1411 Sathyendranath, S., Stuart, V., Nair, A., Oka, K., Nakane, T., Bouman, H., Forget, M.-H.,
1412 Maass, H., and Platt, T.: Carbon-to-chlorophyll ratio and growth rate of phytoplankton in
1413 the sea, *Mar. Ecol. Prog. Ser.*, 383, 73–84, <https://doi.org/10.3354/meps07998>: 2009.

1414 Schmechtig, C., Poteau, A., Claustre, H., D'Ortenzio, F., and Boss, E.: Processing Bio-Argo
1415 chlorophyll a concentration at the DAC Level, *Argo Data Management*, 1–22,
1416 <https://doi.org/10.13155/39468>, 2015.

1417 Schmechtig, C., Poteau, A., Claustre, H., D'Ortenzio, F., Dall'Olmo, G., and Boss, E.:
1418 Processing Bio-Argo particle backscattering at the DAC level Version, *Argo Data*
1419 *Management*, 1–13, <https://doi.org/10.13155/39459>, 2016.

1420 Serret, P., Fernandez, E., Sostres, J. A., and Anadon, R.: Seasonal compensation of microbial
1421 production and respiration in a temperate sea, *Mar. Ecol. Prog. Ser.*, 187, 43–57,
1422 <https://doi.org/10.3354/meps187043>, 1999.

1423 Siegel, D. A., Dickey, T.D., Washburn, L., Hamilton, M. K., and Mitchell, B. G: Optical
1424 determination of particulate abundance and production variations in the oligotrophic
1425 ocean, *Deep-Sea Res. Pt. A*, 36, 211–222, [https://doi.org/10.1016/0198-0149\(89\)90134-](https://doi.org/10.1016/0198-0149(89)90134-9)
1426 9, 1989.

1427 Signorini, S. R., Franz B. A., and McClain C. R.: Chlorophyll variability in the oligotrophic
1428 gyres: mechanisms, seasonality and trends, *Frontiers Mar. Sci.*, 2,
1429 <https://doi.org/10.3389/fmars.2015.00001>, 2015.

1430 Siokou-Frangou, I., Christaki, U., Mazzocchi, M. G., Montresor, M., Ribera d'Alcalá, M.,
1431 Vaqué, D., and Zingone, A.: Plankton in the open Mediterranean Sea: a review,
1432 *Biogeosciences*, 7, 1543–1586, <https://doi.org/10.5194/bg-7-1543-2010>, 2010.

1433 Slade, W. H., and Boss, E.: Spectral attenuation and backscattering as indicators of average
1434 particle size, *Applied Opt.*, 54, 7264–7277, <http://dx.doi.org/10.1364/AO.54.007264>,
1435 2015.

1436 [Smyth, T. J., Pemberton, K. L., Aiken, J., and Geider, R. J.: A methodology to determine](#)
1437 [primary production and phytoplankton photosynthetic parameters from Fast Repetition Rate](#)

1438 [Fluorometry, J. Plank. Res., 26, 11, 1337–1350, https://doi.org/10.1093/plankt/fbh124,](https://doi.org/10.1093/plankt/fbh124)
1439 [2004.](https://doi.org/10.1093/plankt/fbh124)

1440 Stramska, M., and Dickey, T. D.: Variability of bio-optical properties of the upper ocean
1441 associated with diel cycles in phytoplankton population, *J. Geophys. Res.*, 97, 17873–
1442 17887, <https://doi.org/10.1029/92JC01570>, 1992.

1443 Stramski, D., and Kiefer, D.A.: Light scattering by microorganisms in the open ocean. *Prog.*
1444 *Oceanogr.*, 28, 343–383, [https://doi.org/10.1016/0079-6611\(91\)90032-H](https://doi.org/10.1016/0079-6611(91)90032-H), 1991.

1445 Stramski, D., and Reynolds, R. A.: Diel variations in the optical properties of a marine diatom.
1446 *Limnol. Oceanogr.*, 38, 1347–1364, <https://doi.org/10.4319/lo.1993.38.7.1347>, 1993.

1447 Stramski, D., Reynolds, R. A., Kahru, M., and Mitchell, B. G.: Estimation of particulate organic
1448 carbon in the ocean from satellite remote sensing, *Science*, 285, 239–242,
1449 <https://doi.org/10.1126/science.285.5425.239>, 1999.

1450 Stramski, D., Bricaud, A., and Morel, A.: Modeling the inherent optical properties of the ocean
1451 based on the detailed composition of the planktonic community, *Appl. Opt.*, 40, 2929–
1452 2945, <https://doi.org/10.1364/AO.40.002929>, 2001.

1453 Stramski, S., Boss, E., Bogucki, D., and Voss, K. J.: The role of seawater constituents in light
1454 backscattering in the ocean, *Prog. Oceanogr.*, 61, 27–56,
1455 <https://doi.org/10.1016/j.pocean.2004.07.001>, 2004.

1456 Stramski, D., Reynolds, R. A., Babin, M., Kaczmarek, S., Lewis, M. R., Röttgers, R., Sciandra,
1457 A., Stramska, M., Twardowski, M. S., Franz, B. A., and Claustre, H.: Relationships
1458 between the surface concentration of particulate organic carbon and optical properties in
1459 the eastern South Pacific and eastern Atlantic Oceans, *Biogeosciences*, 5, 171–201,
1460 <https://doi.org/10.5194/bg-5-171-2008>, 2008.

1461 [Suggett, D. J., Macintyre, H. L., and Geider, R. J.: Evaluation of biophysical and optical](#)
1462 [determinations of light absorption by photosystem II in phytoplankton, *Limnol. Oceanogr.*](#)
1463 [Methods, 316–332, <https://doi.org/10.4319/lom.2004.2.316>, 2004.](#)

1464 Sullivan, J., Twardowski, M., Ronald, S., Zaneveld, J. V., and Moore, C. C.: Measuring optical
1465 backscattering in water, in: *Light scattering reviews*, edited by Kokhanovsky, A. A.,
1466 Springer, Berlin, 7, 189–224, 2013.

1467 Taillandier, V., Wagener, T., D'Ortenzio, F., Mayot, N., Legoff, H., Ras, J., Coppola, L.,
1468 Pasqueron de Fommervault, O., Schmechtig, C., Diamond, E., Bittig, H., Lefevre, D.,
1469 Leymarie, E., Poteau, A., and Prieur, L.: Hydrography and biogeochemistry dedicated to
1470 the Mediterranean BGC-Argo network during a cruise with RV Tethys 2 in May 2015,
1471 *Earth Syst. Sci. Data*, 10, 627–641, <https://doi.org/10.5194/essd-10-627-2018>, 2018.

1472 Turley, C. M., Bianchi, M., Christaki, U., Conan, P., Harris, J. R. W., Psarra, S., Ruddy, G.,
1473 Stutt, E. D., Tselepidis, A., Van Wambeke, F.: Relationship between primary producers
1474 and bacteria in an oligotrophic sea - The Mediterranean and biogeochemical implications,
1475 *Mar. Ecol. Progr. Ser.*, 193, 11–18, <https://doi.org/10.3354/meps193011>, 2000.

1476 Twardowski, M. S., Boss, E., Macdonald, J. B., Pegau, W. S., Barnard, A. H., and Zaneveld, J.
1477 R. V.: A model for estimating bulk refractive index from the optical backscattering ratio
1478 and the implications for understanding particle composition in case I and case II waters.
1479 *J. Geophys. Res.*, 106, 14129–14142, <https://doi.org/10.1029/2000JC000404>, 2001.

1480 Uitz, J., Claustre, H., Morel, A., and Hooker, S. B.: Vertical distribution of phytoplankton
1481 communities in open ocean: An assessment based on surface chlorophyll, *J. Geophys.*
1482 *Res.*, 111, 1–23, <https://doi.org/10.1029/2005JC003207>, 2006.

1483 Uitz, J., Claustre, H., Gentili, B., and Stramski, D.: Phyto- plankton class-specific primary
1484 production in the world's oceans: Seasonal and interannual variability from satellite

1485 observations, *Global Biogeochem. Cy.*, 24, 1–19, <https://doi.org/10.1029/2009gb003680>,
1486 2010.

1487 Uitz, J., Stramski, D., Gentili, B., D’Ortenzio, F., and Claustre, H.: Estimates of phytoplankton
1488 class-specific and total primary production in the Mediterranean Sea from satellite ocean
1489 color observations, *Global Biogeochem. Cy.*, 26, 1–10,
1490 <https://doi.org/10.1029/2011gb004055>, 2012.

1491 Ulloa, O., Sathyendranath, S., and Platt, T.: Effect of the particle-size distribution on the
1492 backscattering ratio in seawater, *Appl. Opt.*, 33, 7070–7077,
1493 <https://doi.org/10.1364/AO.33.007070>, 1994.

1494 Vaulot, D., and Marie, D.: Diel variability of photosynthetic picoplankton in the equatorial
1495 Pacific, *J. Geophys. Res.*, 104, 3297–3310, <https://doi.org/10.1029/98JC01333>, 1999.

1496 Vidussi, F., Claustre, H., Manca, B. B., Luchetta, A., and Marty, J.-C.: Phytoplankton pigment
1497 distribution in relation to upper thermocline circulation in the eastern Mediterranean Sea
1498 during winter, *J. Geophys. Res.*, 106, 19,939–19,956,
1499 <https://doi.org/10.1029/1999JC000308>, 2001.

1500 Westberry, T., Behrenfeld, M. J., Siegel, D. A., and Boss, E.: Carbon-based primary
1501 productivity modeling with vertically resolved photoacclimation, *Global Biogeochem. Cy.*,
1502 222, 1–18, <https://doi.org/10.1029/2007GB003078>, 2008.

1503 Westberry, T. K., Dall’Olmo, G., Boss, E., Behrenfeld, M., and Moutin, T.: Coherence of
1504 particulate beam attenuation and backscattering coefficients in diverse open ocean
1505 environments, *Opt. Express*, 18, 15,419–15,425, <https://doi.org/10.1364/OE.18.015419>,
1506 2010.

1507 White, A. E., Barone, B., Letelier, R. M., and Karl, D. M.: Productivity diagnosed from the diel
1508 cycle of particulate carbon in the North Pacific Subtropical Gyre, *Geophys. Res. Lett.*,
1509 44, 3752–3760, <https://doi.org/10.1002/2016GL071607>, 2017.

1510 Whitmire, A. L., Boss, E., Cowles, T. J., and Pegau, W. S.: Spectral variability of the particulate
1511 backscattering ratio, *Opt. Express* 15, 7019–7031,
1512 <https://doi.org/10.1364/OE.15.007019>, 2007.

1513 Williams, P. J. le B., and Jenkinson, N.W.: A transportable microprocessor controlled precise
1514 Winkler titration suitable for field station and shipboard use, *Limnol. Oceanogr.*, 27, 576–
1515 584, <https://doi.org/10.4319/lo.1982.27.3.0576>, 1982.

1516 Williams, P. J. le B., and Purdie, D. A.: In vitro and in situ derived rates of gross production,
1517 net community production and respiration of oxygen in the oligotrophic subtropical gyre
1518 of the North Pacific Ocean, *Deep-Sea Res. Pt. A*, 38, 891–910,
1519 [https://doi.org/10.1016/0198-0149\(91\)90024-A](https://doi.org/10.1016/0198-0149(91)90024-A), 1991.

1520 Williams, P. J. le B.: On the definition of plankton production terms, in: *Measurement of*
1521 *primary production from the molecular to the global scale*, edited by Li, W. K., and
1522 Maestrini, S. I., ICES mar. Sci. Symp, Copenhagen, 9–19, 1993.

1523 Williams, P. J. le B., Morris, P. J., and Karl, D. M.: Net community production and metabolic
1524 balance at the oligotrophic ocean site, station ALOHA, *Deep-Sea Res. Pt. I*, 51, 1563–
1525 1578, <https://doi.org/10.1016/j.dsr.2004.07.001>, 2004.

1526 Xing, X., Claustre, H., Blain, S., D'Ortenzio, F., Antoine, D., Ras, J., Guinet, C.: Quenching
1527 correction for in vivo chlorophyll fluorescence acquired by autonomous platforms: A case
1528 study with instrumented elephant seals in the Kerguelen region (Southern Ocean),
1529 *Limnol. Oceanogr.-Meth.*, 10, 483–495, <https://doi.org/10.4319/lom.2012.10.483>, 2012.

- 1530 Yentsch, C. S., and Phinney, D. A.: A bridge between ocean optics and microbial ecology.
1531 *Limnol. Oceanogr.*, 34, 1694–1705, <https://doi.org/10.4319/lo.1989.34.8.1694>, 1989.
- 1532 Zhang, X., Hu, L., and He, M.-X.: Scattering by pure seawater: Effect of salinity, *Opt. Express*,
1533 17, 5698–5710, <https://doi.org/10.1364/OE.17.005698>, 2009.

Figure captions

Figure 1: Trajectories of the two BGC-Argo profiling floats fLig (WMO6901776) and flon (WMO6902828) deployed respectively in the Ligurian Sea (green) and the Ionian Sea (blue), superimposed onto a 9-km resolution summer climatology of surface chlorophyll *a* concentration (in mg m^{-3}) derived from MODIS Aqua ocean color measurements. The asterisk-shaped symbol indicates the geographic location of the BOUSSOLE site.

Figure 2: Schematic representation of the diel variations of the depth-integrated bio-optical properties converted to POC biomass (*B*) and the sampling strategies employed in the (a) Ligurian Sea and (b) Ionian Sea. The diamond-shaped symbols indicate schematically the float profile times, labeled with time stamps associated with sunrise (sr), noon (n), sunset (ss) and midnight (m), with the corresponding POC biomass estimated within the considered layer (e.g., $B(t_{sr})$, etc.). The numeric subscripts (+1, +2, +4 or +5) indicate the number of days since the first profile of the summertime time series.

Figure 3: Time series of the vertical distribution of the *Chl* (a and d), b_{bp} (b and e), c_p (d and f), and instantaneous midday PAR (d and h), in the Ligurian Sea (left) and the Ionian Sea (right). The euphotic depth (Z_{eu} ; white line), the Mixed Layer Depth (MLD; black line), the depth of the SCM (magenta line), and the depth of the isopycnal 28.85 expressed as σ_t (blue line), are superimposed onto the bio-optical timeseries. The dashed lines indicate the dates at which the c_p and the b_{bp} values in the SCM layer reach a minimum.

a supprimé: and

Figure 4: Temporal evolution of *Chl* (a and d), c_p (b and e), and b_{bp} (c and f) in the surface (dark green) and SCM (red) layers for the Ligurian Sea (left) and the Ionian Sea (right). The dashed lines indicate the dates when the values of c_p and b_{bp} in the SCM layer reach a minimum.

Figure 5: Example of the variations of the c_p (a) and b_{bp} (b) coefficients at the daily time scale in the Ionian Sea in the SCM layer during the interval from September 2 to September 6, 2017. The grey shaded area indicates the nighttime.

Figure 6: Comparison of the biological production integrated within the euphotic layer, derived from the diel cycle of c_p (blue) or b_{bp} (yellow) or computed using the bio-optical primary production model of Morel (1991) (purple) for the Ligurian Sea (a) and the Ionian Sea (b).

Figure 7: Temporal evolution of the POC and community production derived from the diel cycle of c_p in the Ligurian Sea (a–b) and the Ionian Sea (c–d) and integrated in three different

layers of the water column: surface (dark green), euphotic (light blue) and SCM (red) layers. The dotted lines indicate the dates when c_p in the SCM layer reaches a minimum.

Figure 8: Depth-interpolated timeseries of the relative contributions (%) to the chlorophyll *a* concentration of the micro- (a and d), nano- (b and e) and picophytoplankton (c and h) derived from HPLC pigment determinations in the Ligurian Sea (BOUSSOLE site; left) and Ionian Sea (PEACETIME cruise; right). The pigment data were collected at the BOUSSOLE site in the same region and at the same time period as the fLig float deployment (see text section 2.1). The flon float was deployed concurrently to sampling for HPLC pigments at the PEACETIME ION station. Pigment data collected at ION over four days prior to float deployment are shown. [As an indication, the depths of the euphotic depth \(\$Z_{eu}\$; white dashed line\), mixed layer \(MLD; black dashed line\) and SCM \(magenta dashed line\) derived from the BGC-Argo float measurements, as in Fig. 3, are overlaid onto the pigment data.](#)

Figure 9: Temporal evolution of the bio-optical ratios of b_{bp} / c_p (a), c_p / Chl (b) and b_{bp} / Chl (c) in the SCM layer for the Ligurian Sea (left) and the Ionian Sea (right). The dotted lines indicate the dates when the values of c_p in the SCM layer reach a minimum.

Figure 10: Time series of the daily-integrated photosynthetically available radiation (PAR) at the SCM level in the Ligurian Sea (a) and the Ionian Sea (b). The horizontal grey line shows the median of each time series. The dotted lines indicate the dates at which the values of c_p in the SCM layer reach a minimum.

Table 1: POC-to- c_p relationships from the literature, with POC and c_p in units of mg m^{-3} and m^{-1} , respectively.

Reference	Region	Relationship
Marra et al. (1995)	North Atlantic	$\text{POC} = 367 c_p(660) + 31.2$
Claustre et al. (1999)	Equatorial Pacific	$\text{POC} = 501.81 c_p(660) + 5.33$
Oubelkheir et al. (2005)	Mediterranean	$\text{POC} = 574 c_p(555) - 7.4$
Behrenfeld & Boss (2006)	Equatorial Pacific	$\text{POC} = 585.2 c_p(660) + 7.6$
Gardner et al. (2006)	Global Ocean	$\text{POC} = 381 c_p(660) + 9.4$
Stramski et al. (2008)	Pacific and Atlantic, including upwelling	$\text{POC} = 661.9 c_p(660) - 2.168$
Loisel et al (2011)	Mediterranean	$\text{POC} = 404 c_p(660) + 29.25$
Cetinić et al. (2012)	North Atlantic	$\text{POC} = 391 c_p(660) - 5.8$

Table 2: POC-to- b_{bp} relationships from the literature, with POC and b_{bp} in units of mg m^{-3} and m^{-1} , respectively.

Reference	Region	Relationship
Stramski et al. (2008)	Pacific and Atlantic, including upwelling	$\text{POC} = 71002 b_{bp}(555) - 5.5$
Loisel et al (2011)	Mediterranean	$\text{POC} = 37550 b_{bp}(555) + 1.3$
Cetinić et al. (2012)	North Atlantic	$\text{POC} = 35422 b_{bp}(700) - 14.4$

Table 3: Mean and range (%) in relative daily variations ($\bar{m}\Delta$ and $\bar{r}\Delta$, respectively) in the diel cycle of c_p and b_{bp} computed for each float over the entire time series, for the two considered regions and in the surface ($0-Z_{pd}$) and SCM layers of the water column.

Region		Surface layer		SCM layer	
		Δc_p	Δb_{bp}	Δc_p	Δb_{bp}
Ligurian Sea	$\bar{m}\Delta$	12.7	-2.3	14.5	3.8
	$\bar{r}\Delta$	256.7	28.5	194.8	107.8
Ionian Sea	$\bar{m}\Delta$	0.55	0.23	1.16	0.06
	$\bar{r}\Delta$	54.4	21.2	102.4	57.3

Table 4: Estimates of primary and community production (in units of $\text{gC m}^{-2} \text{d}^{-1}$) from the literature in areas of the Mediterranean Sea comparable, when possible, to the considered study regions.

Primary production					
Method	Reference	Area	Period	Layer	Estimate
Ocean color-coupled bio-optical model	Morel & André (1991)	Western basin	1981	0– Z_{eu}	0.26
	Antoine et al. (1995)	Whole basin	1979-1981	0–1.5 Z_{eu}	0.34
	Bosc et al. (2004)	Western basin	1998-2001	0–1.5 Z_{eu}	0.45
	-	Eastern basin	-	-	0.33
	Uitz et al. (2012)	Bloom region	May-Aug 1998-2007	0–1.5 Z_{eu}	0.26–0.82
	-	No bloom region	-	-	0.22–0.69
Biogeochemical model	Lacroix & Nival (1998)	Ligurian Sea		0–200 m	0.13
	Allen et al. (2002)	Ligurian Sea		0– Z_{eu}	0.33
	-	Ionian Sea		-	0.14
In-situ ^{14}C measurements	Minas (1970)	Northwestern basin	1961-1965	Surface	0.21
	Magazzu & Decembrini (1995)	Ionian Sea	1983-1992	0– Z_{eu}	0.22
	Turley et al. (2000)	Ligurian Sea	Oct 1997, Apr-May 1998	0– Z_{eu}	0.5
	Marañón et al. (2021)	Ionian Sea	May 2017	0–200 m	0.19
Gross community production					
Method	Reference	Area	Period	Layer	Estimate
c_p diel cycle-based method	Barnes & Antoine (2014)	Ligurian Sea	May-Aug 2006-2011	0– Z_{eu}	0.8–1.5

Table 5: Comparison of the mean rates \pm SD ($\text{gC m}^{-2} \text{d}^{-1}$) of the community production integrated within the euphotic layer, derived from the application of the bio-optical diel cycle-based method to the c_p measurements, using different bio-optical relationships from the literature for converting the c_p values into POC biomass.

Reference	Ligurian Sea	Ionian Sea
Marra et al. (1995)	0.89 \pm 0.84	0.35 \pm 0.09
Claustre et al. (1999)	1.22 \pm 1.16	0.48 \pm 0.12
Oubelkheir et al. (2005)	1.18 \pm 1.13	0.46 \pm 0.11
Behrenfeld & Boss (2006)	1.43 \pm 1.35	0.56 \pm 0.14
Gardner et al. (2006)	0.93 \pm 0.88	0.36 \pm 0.09
Stramski et al. (2008)	1.62 \pm 1.54	0.63 \pm 0.16
Loisel et al. (2011)	0.98 \pm 0.92	0.38 \pm 0.10
Cetinić et al. (2012)	0.96 \pm 0.91	0.37 \pm 0.09

Table 6: Community production mean rates \pm SD ($\text{gC m}^{-2} \text{d}^{-1}$) derived from the application of the bio-optical diel cycle-based method to the c_p measurements in the two considered regions. The production rates are integrated within the surface, subsurface maximum (SCM), and euphotic layers.

Variable	Ligurian Sea			Ionian Sea		
	Euphotic	Surface	SCM	Euphotic	Surface	SCM
POC ($\text{gC m}^{-2} \text{d}^{-1}$)	3.67 \pm 1.11	0.36 \pm 0.17	3.86 \pm 1.20	1.88 \pm 0.24	0.34 \pm 0.14	0.93 \pm 0.31
GCP ($\text{gC m}^{-2} \text{d}^{-1}$)	1.18 \pm 1.13	0.29 \pm 0.33	0.96 \pm 1.28	0.46 \pm 0.11	0.11 \pm 0.04	0.14 \pm 0.39

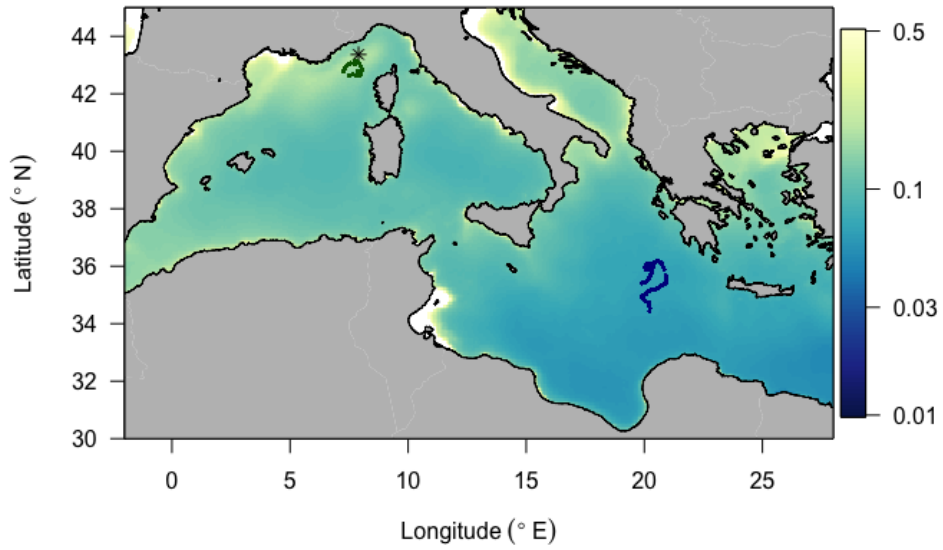


Figure 1: Trajectories of the two BGC-Argo profiling floats fLig (WMO6901776) and flon (WMO6902828) deployed respectively in the Ligurian Sea (green) and the Ionian Sea (blue), superimposed onto a 9-km resolution summer climatology of surface chlorophyll *a* concentration (in mg m⁻³) derived from MODIS Aqua ocean color measurements. The asterisk-shaped symbol indicates the geographic location of the BOUSSOLE site.

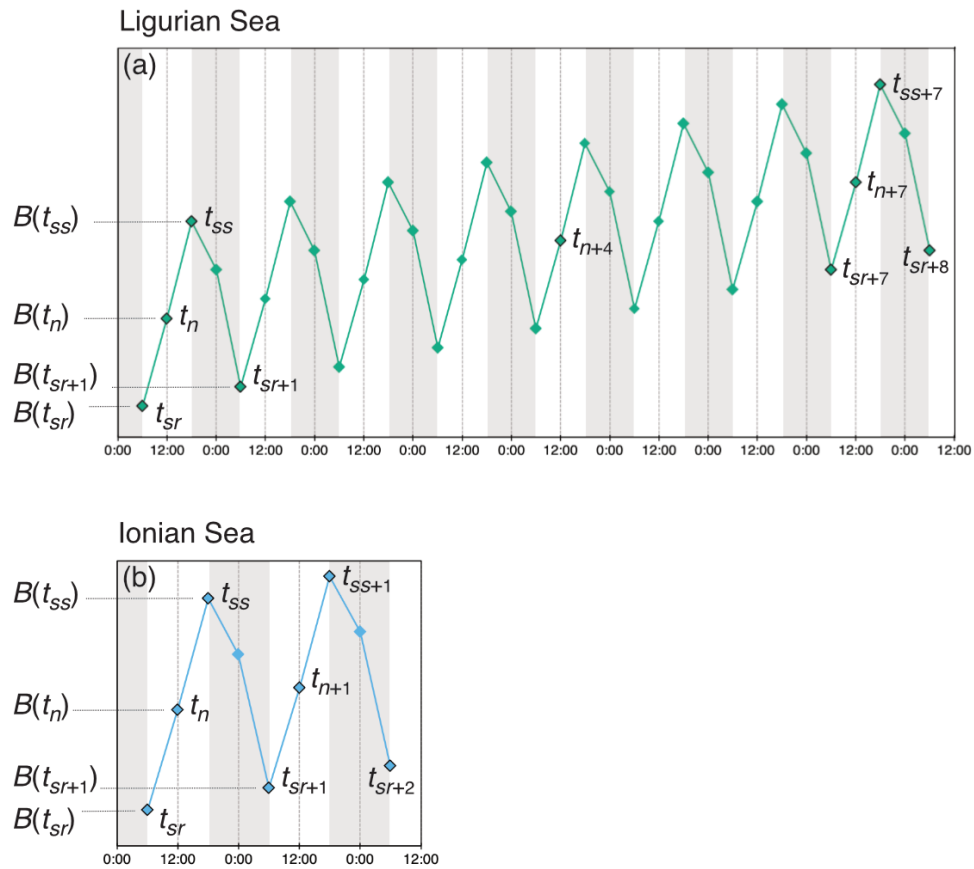


Figure 2: Schematic representation of the diel variations of the depth-integrated bio-optical properties converted to POC biomass (B) and the sampling strategies employed in the (a) Ligurian Sea and (b) Ionian Sea. The diamond-shaped symbols indicate schematically the float profile times, labeled with time stamps associated with sunrise (sr), noon (n), sunset (ss) and midnight (m), with the corresponding POC biomass estimated within the considered layer (e.g., $B(t_{sr})$, etc.). The numeric subscripts (+1, +2, +4 or +5) indicate the number of days since the first profile of the summertime time series.

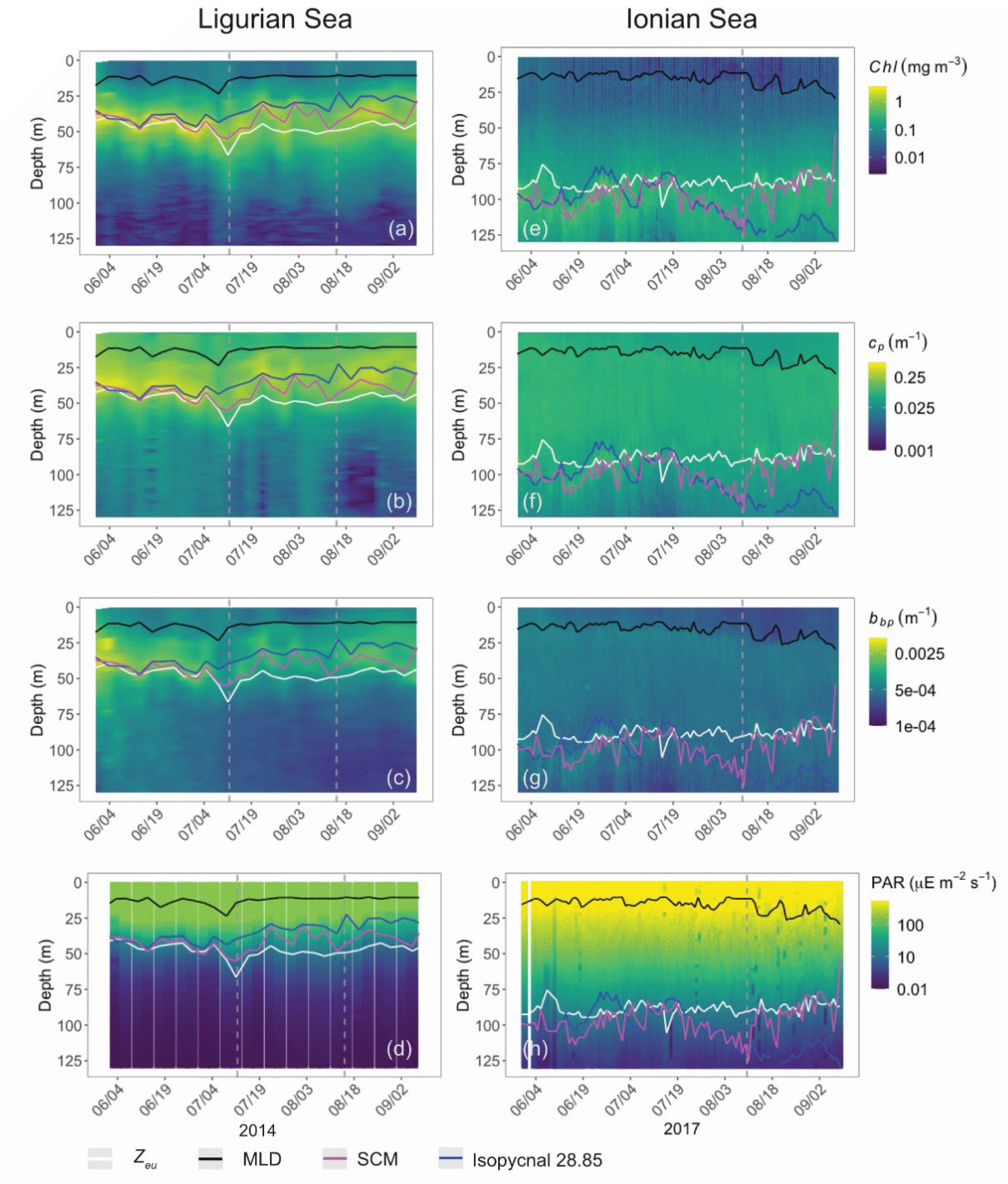


Figure 3: Time series of the vertical distribution of the Chl (a and d), b_{bp} (b and e), c_p (d and f), and instantaneous midday PAR (d and h), in the Ligurian Sea (left) and the Ionian Sea (right). The euphotic depth (Z_{eu} ; white line), the Mixed Layer Depth (MLD; black line), the depth of the SCM (magenta line), and the depth of the isopycnal 28.85 expressed as (blue line), are superimposed onto the bio-optical timeseries. The dashed lines indicate the dates at which the c_p and the b_{bp} values in the SCM layer reach a minimum.

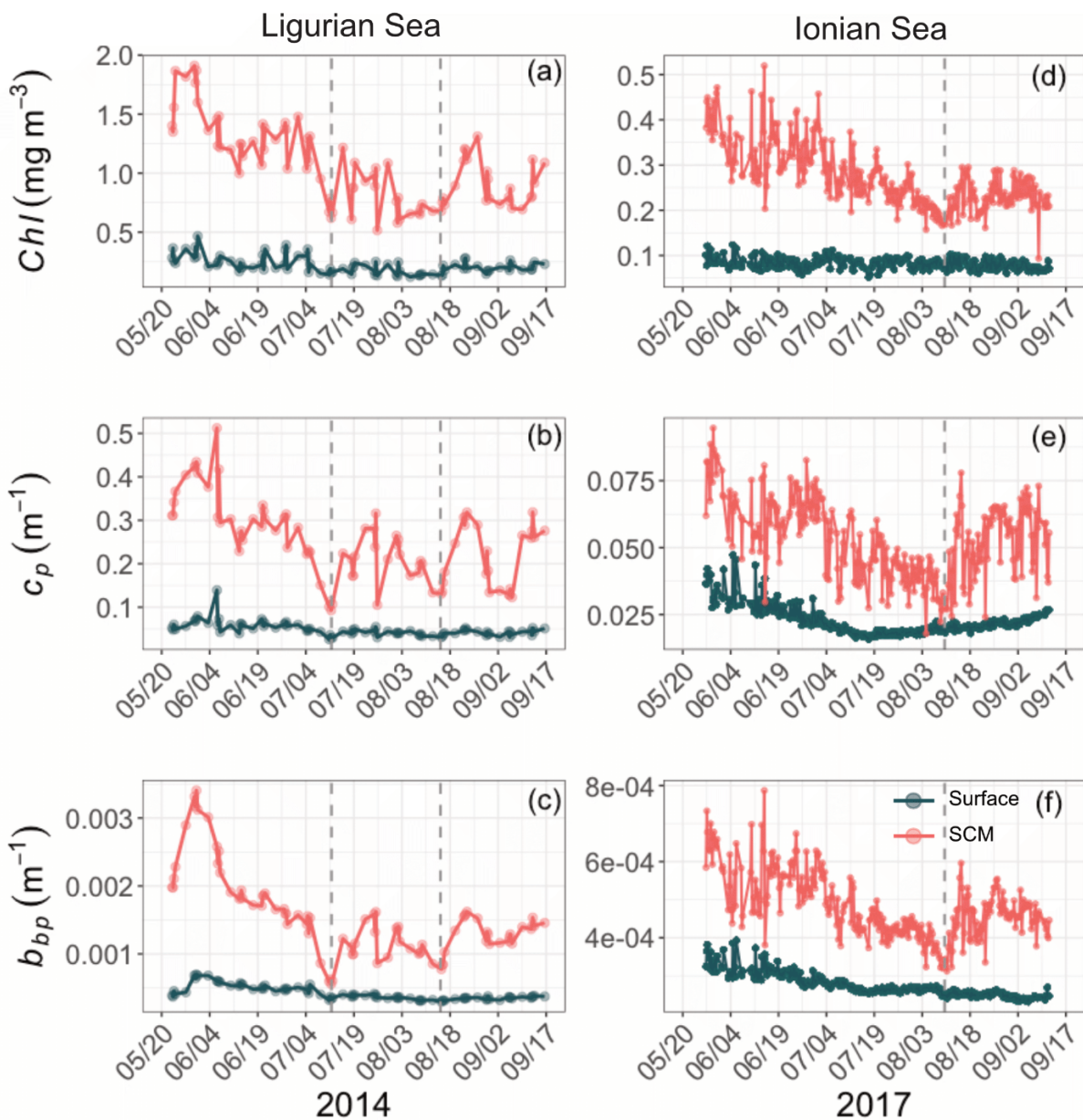


Figure 4: Temporal evolution of Chl (a and d), c_p (b and e), and b_{bp} (c and f) in the surface (dark green) and SCM (red) layers for the Ligurian Sea (left) and the Ionian Sea (right). The dashed lines indicate the dates when the values of c_p and b_{bp} in the SCM layer reach a minimum.

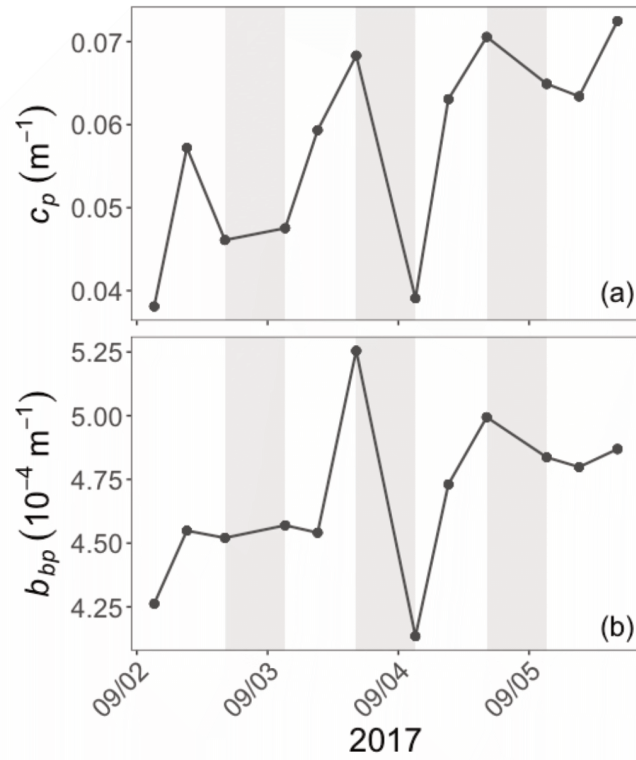


Figure 5: Example of the variations of the c_p (a) and b_{bp} (b) coefficients at the daily time scale in the Ionian Sea in the SCM layer during the interval from September 2 to September 6, 2017. The grey shaded area indicates the nighttime.

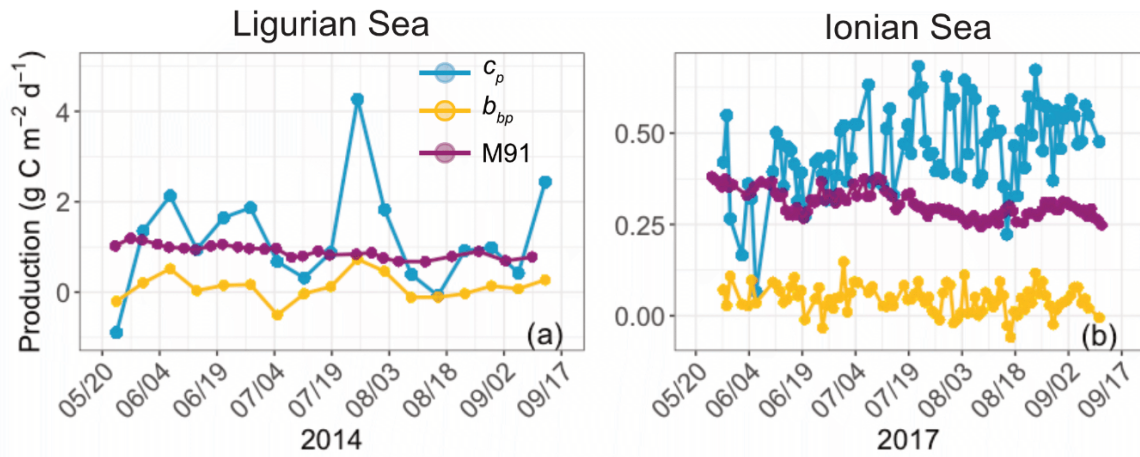


Figure 6: Comparison of the biological production integrated within the euphotic layer, derived from the diel cycle of c_p (blue) or b_{bp} (yellow) or computed using the bio-optical primary production model of Morel (1991) (purple) for the Ligurian Sea (a) and the Ionian Sea (b).

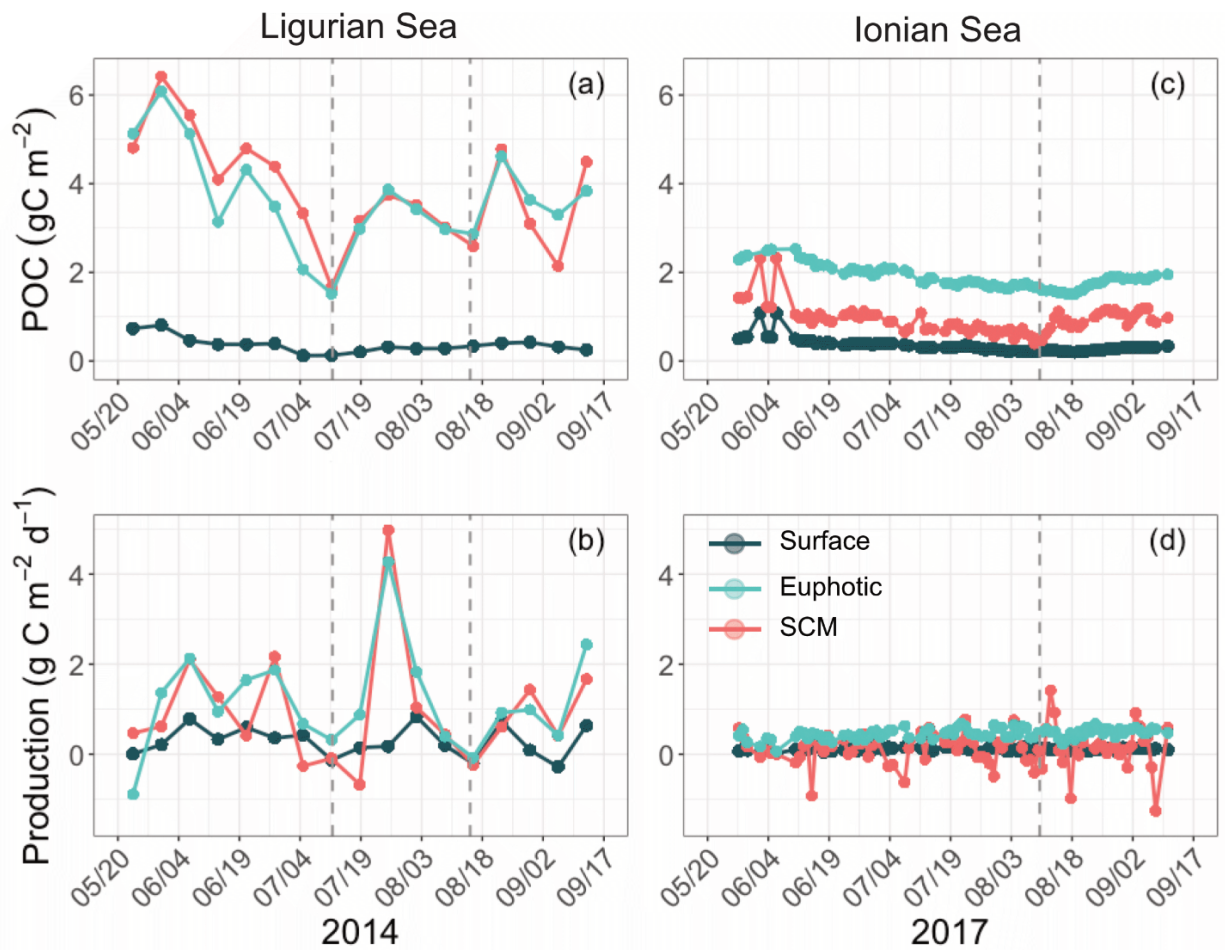


Figure 7: Temporal evolution of the POC and community production derived from the diel cycle of c_p in the Ligurian Sea (a–b) and the Ionian Sea (c–d) and integrated in three different layers of the water column: surface (dark green), euphotic (light blue) and SCM (red) layers. The dotted lines indicate the dates when c_p in the SCM layer reaches a minimum.

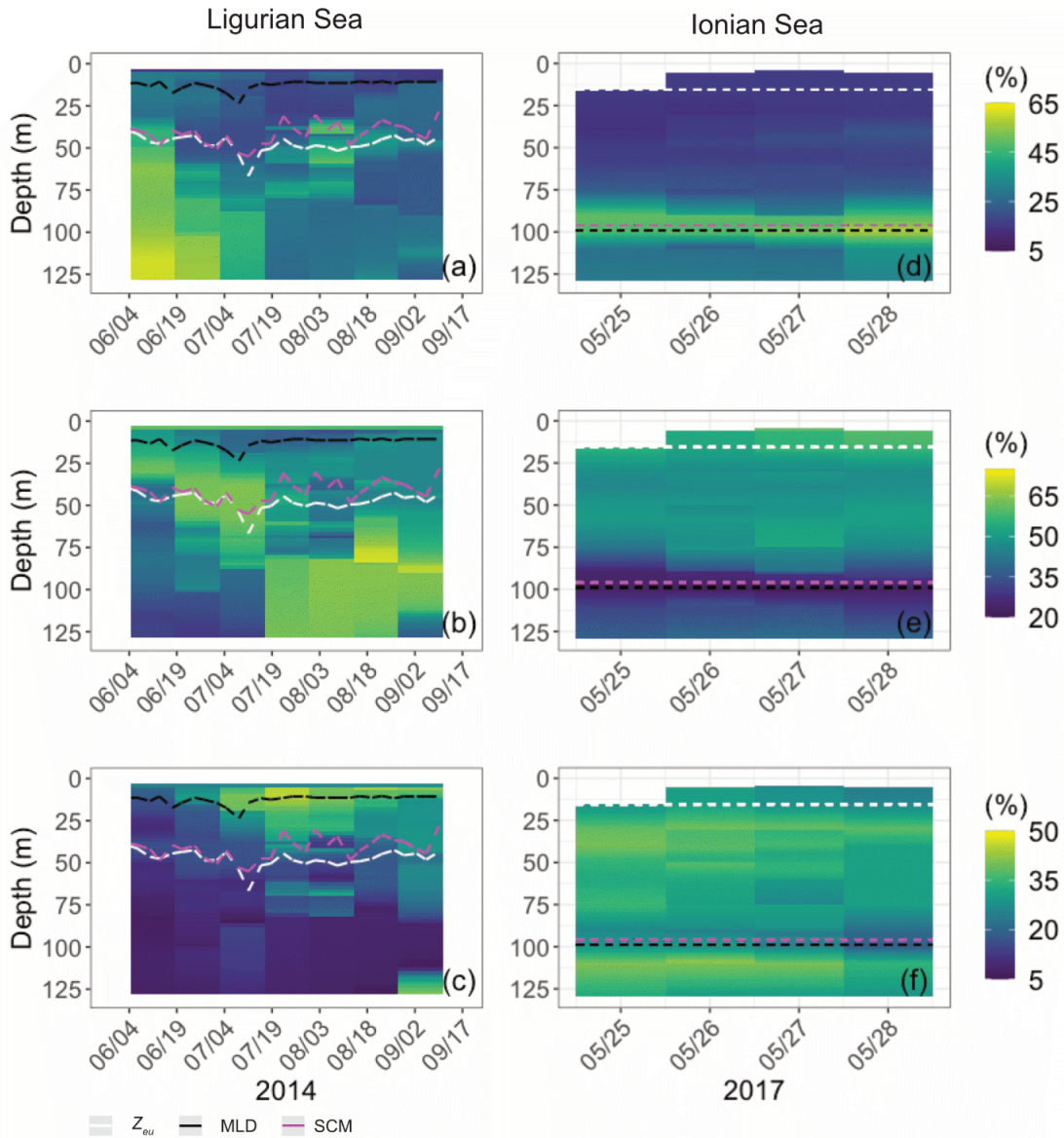


Figure 8: Depth-interpolated timeseries of the relative contributions (%) to the chlorophyll *a* concentration of the micro- (a and d), nano- (b and e) and picophytoplankton (c and h) derived from HPLC pigment determinations in the Ligurian Sea (BOUSSOLE site; left) and Ionian Sea (PEACETIME cruise; right). The pigment data were collected at the BOUSSOLE site in the same region and at the same time period as the fLig float deployment (see text section 2.1). The flon float was deployed concurrently to sampling for HPLC pigments at the PEACETIME ION station. Pigment data collected at ION over four days prior to float deployment are shown. As an indication, the depths of the euphotic depth (Z_{eu} ; white dashed line), mixed layer (MLD; black dashed line) and SCM (magenta dashed line) derived from the BGC-Argo float measurements, as in Fig. 3, are overlaid onto the pigment data.

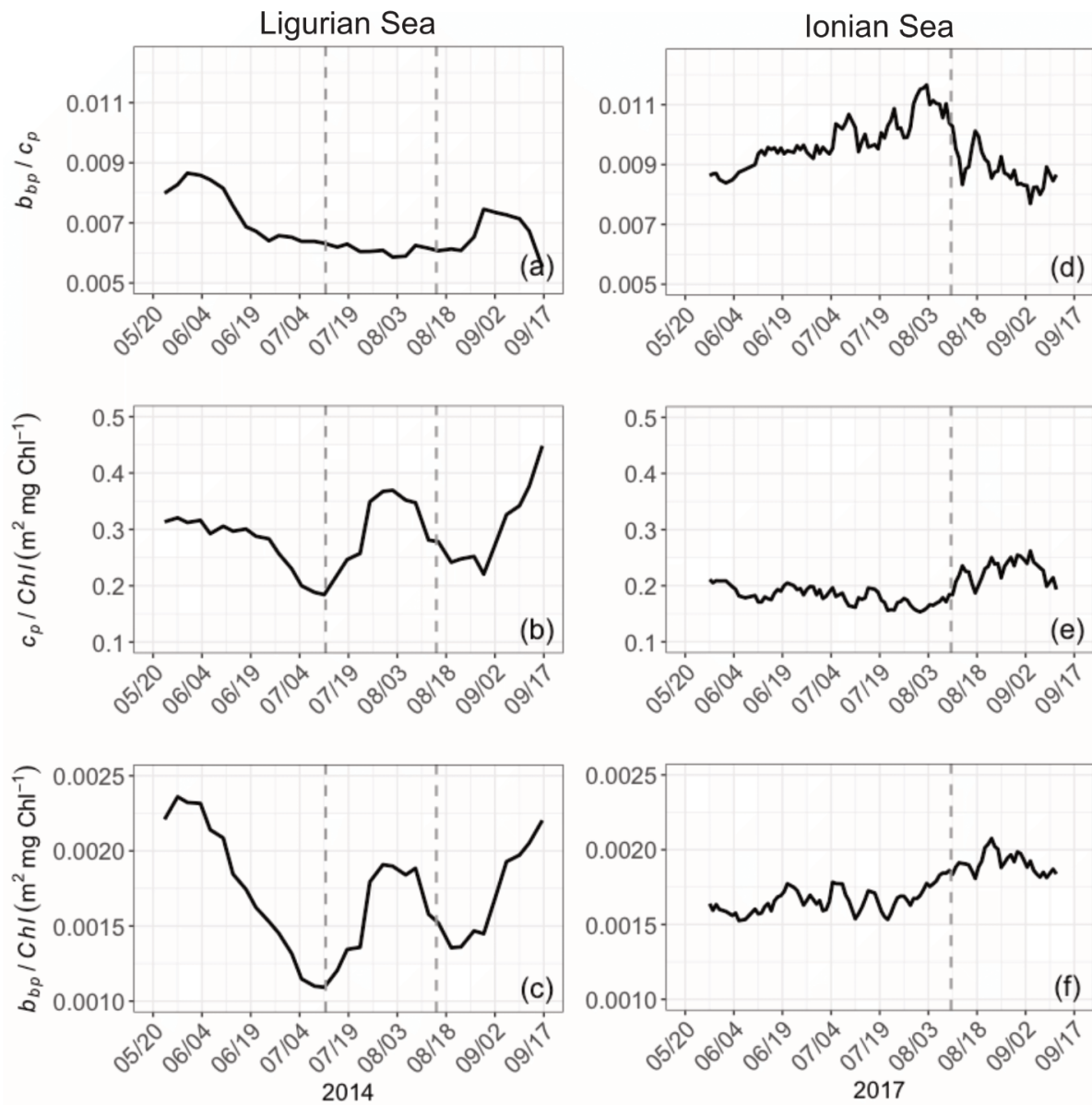


Figure 9: Temporal evolution of the bio-optical ratios of b_{bp} / c_p (a), c_p / Chl (b) and b_{bp} / Chl (c) in the SCM layer for the Ligurian Sea (left) and the Ionian Sea (right). The dotted lines indicate the dates when the values of c_p in the SCM layer reach a minimum.

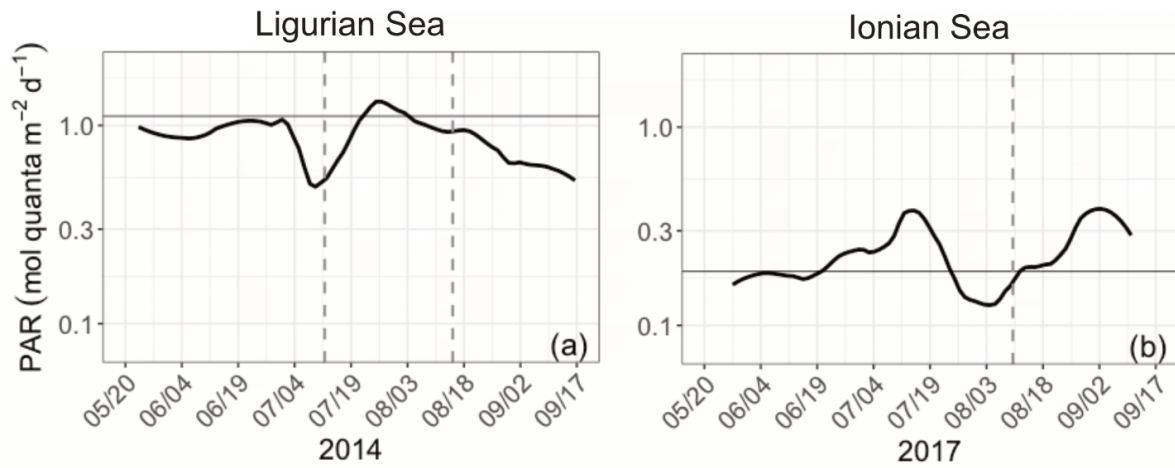


Figure 10: Time series of the daily-integrated photosynthetically available radiation (PAR) at the SCM level in the Ligurian Sea (a) and the Ionian Sea (b). The horizontal grey line shows the median of each time series. The dotted lines indicate the dates at which the values of c_p in the SCM layer reach a minimum.

APPENDIX A

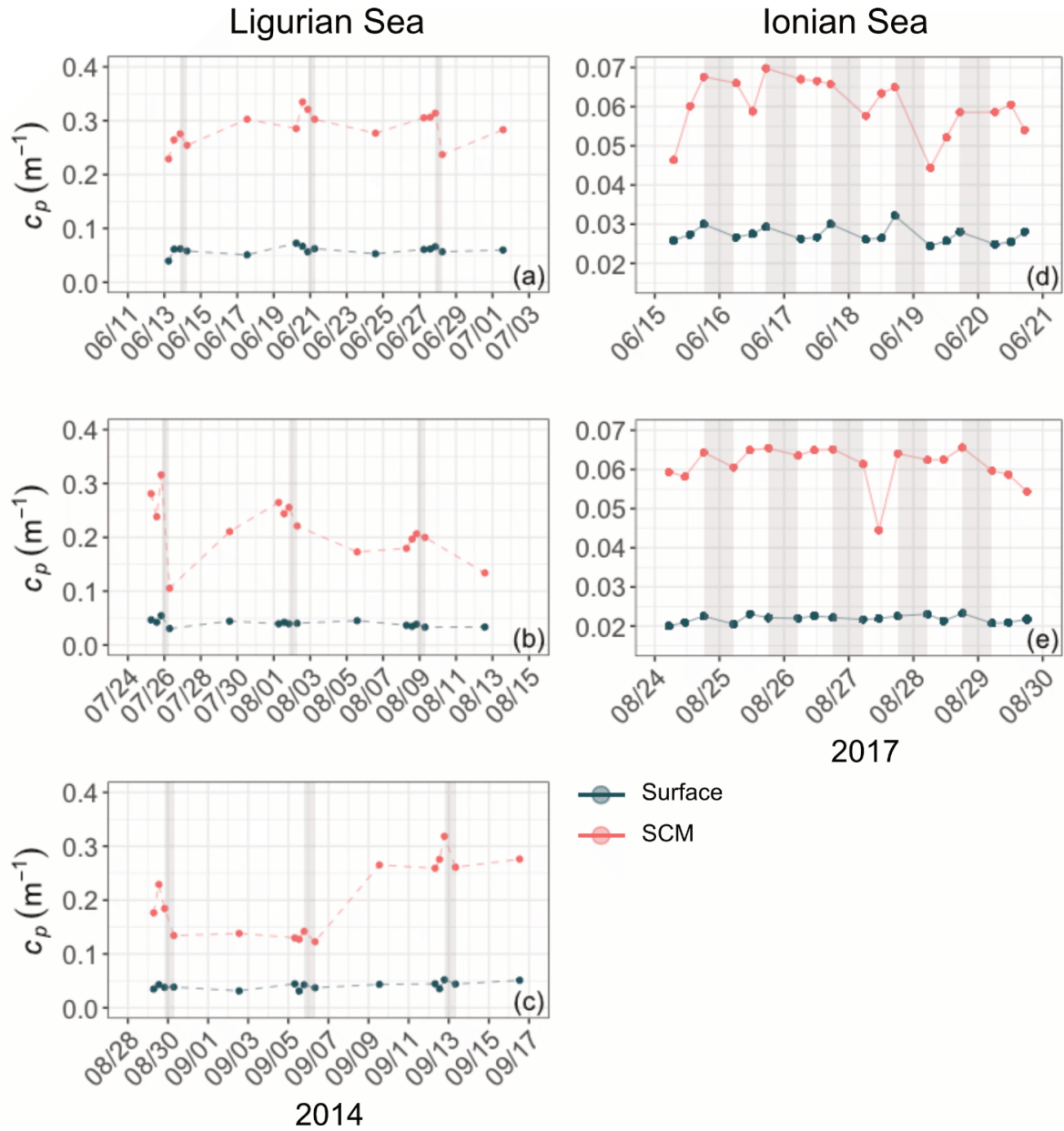


Figure A1: Example of time series of the c_p coefficient in the surface (red) and SCM (dark green) layers, chosen within the time periods indicated by the dashed lines in Figs 3-4, from May 24 to July 14, 2014 (a), July 14 to August 16, 2014 (b), and August 16 to September 13, 2014 for the Ligurian Sea (left), and from May 28 to August 11, 2017 (d) and August 11 to September 11, 2017 (e) for the Ionian Sea (right).

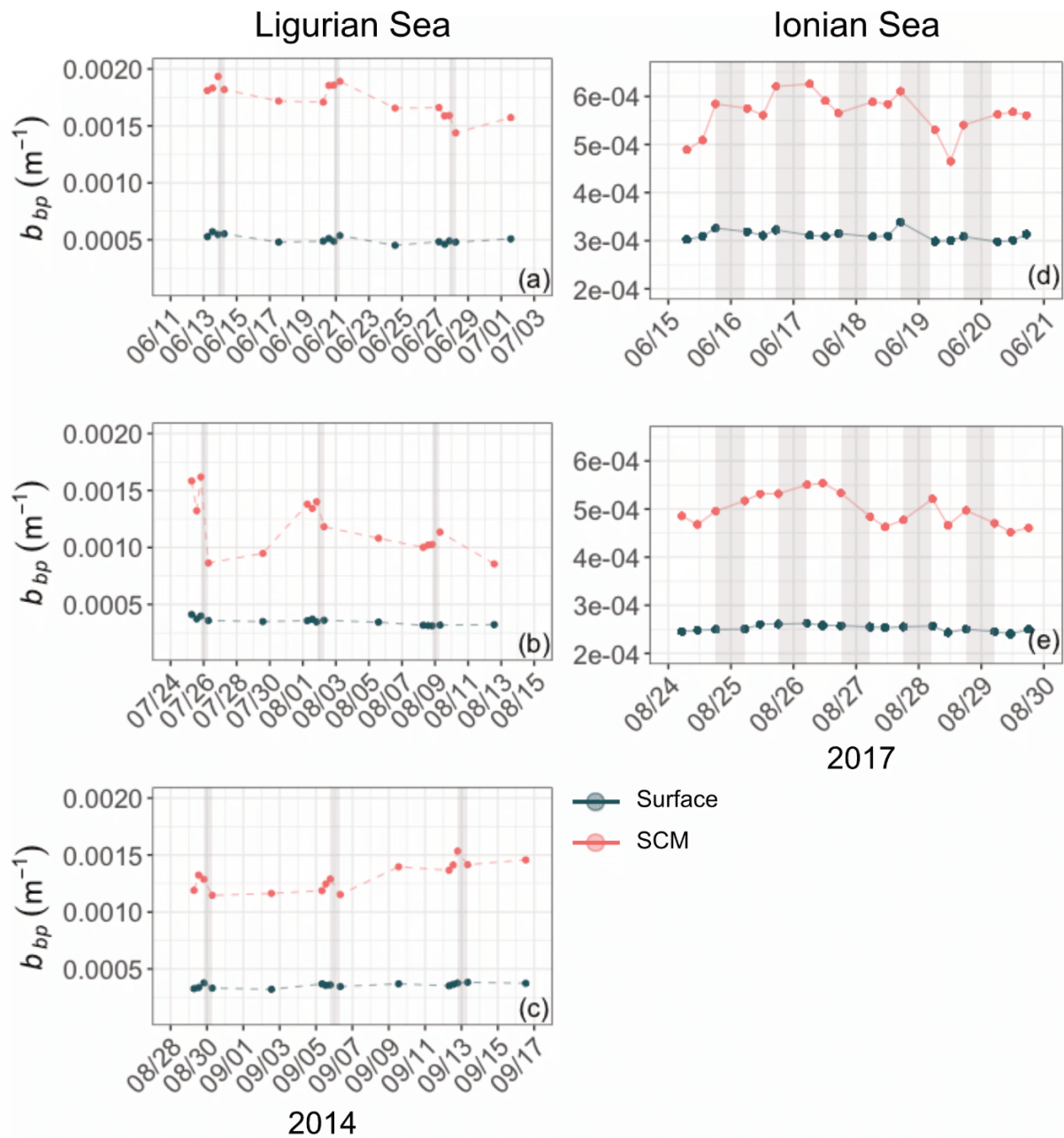


Figure A2: Example of time series of the b_{bp} coefficient in the surface (red) and SCM (dark green) layers, chosen within the time periods indicated by the dashed lines in Figs 3-4, from May 24 to July 14, 2014 (a), July 14 to August 16, 2014 (b), and August 16 to September 13, 2014 for the Ligurian Sea (left), and from May 28 to August 11, 2017 (d) and August 11 to September 11, 2017 (e) for the Ionian Sea (right).

APPENDIX B

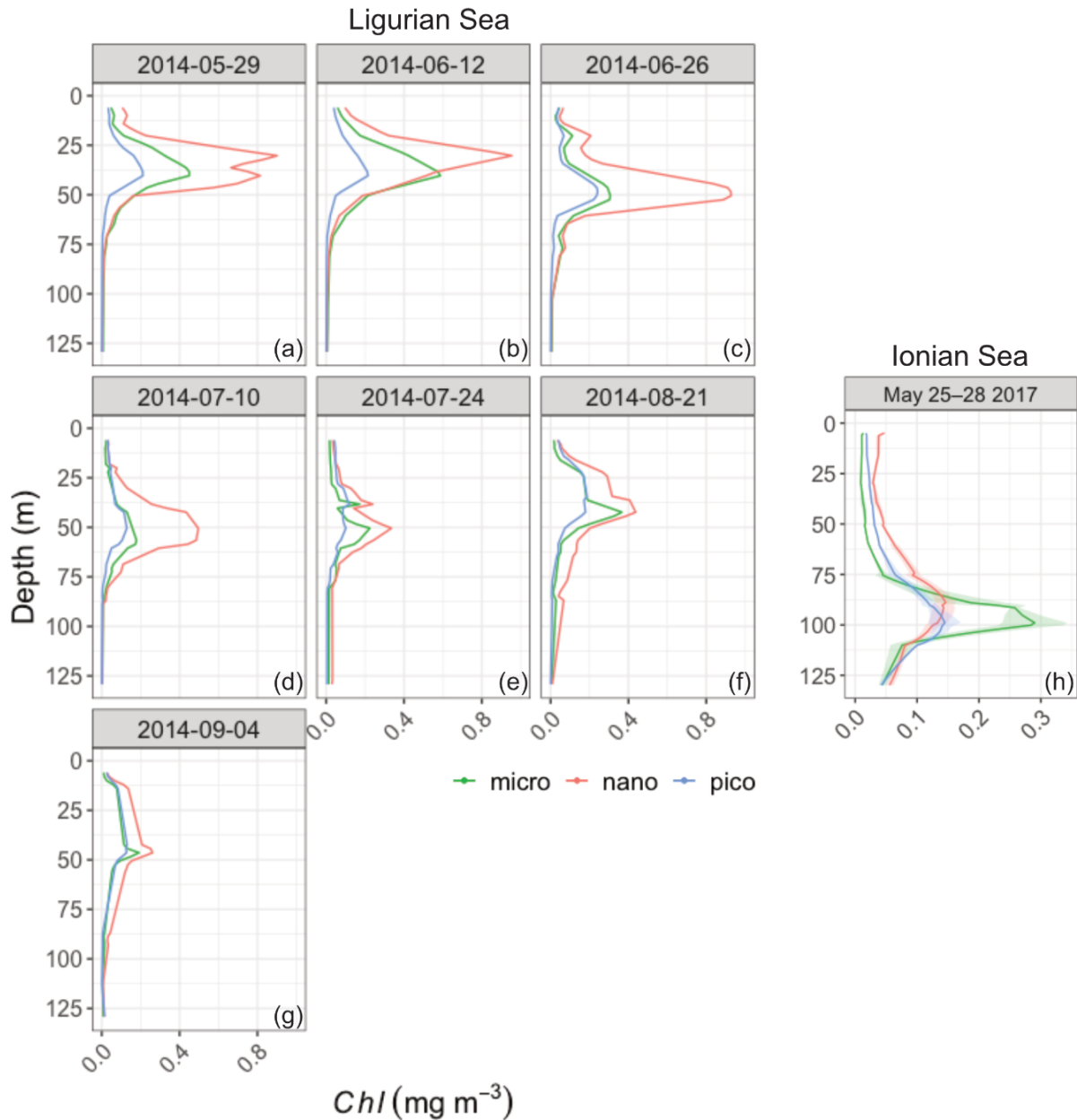


Figure B1: Vertical distribution of the chlorophyll *a* concentration of the micro- (green), nano- (red) and picophytoplankton (blue) derived from HPLC pigment determinations in the Ligurian Sea (BOUSSOLE site; a–h) and the Ionian Sea (PEACETIME cruise; i). For the Ionian Sea the solid line shows the mean value and the shaded area the standard deviation, calculated over a 4-day window (May 25–28, 2017).